Summer 8-11-2017

Nanocellulose Fibers as a Potential Material for Orthopedic Implantation Application

David Gregg Holomakoff
david.holomakoff@maine.edu

NANOCELLULOSE FIBERS AS A POTENTIAL MATERIAL FOR ORTHOPEDIC IMPLANTATION APPLICATION

By

David G. Holomakoff

B.S. University of Maine, 2014

A THESIS

Submitted in Partial Fulfillment of the

Requirement for the Degree of

Master of Science

(in Biological Engineering)

The Graduate School

The University of Maine

August 2017

Advisory Committee:

Dr. Michael Mason, Professor of Biological and Chemical Engineering, Advisor

Dr. Doug Bousfield, Professor of Biological and Chemical Engineering

Dr. Paul Millard, Professor of Biological and Chemical Engineering

Dr. Ian Dickey, Orthopedic Surgeon, Adjunct Professor, Chair of External Advisory Board - Bioengineering

NANOCELLULOSE FIBERS AS A POTENTIAL MATERIAL FOR ORTHOPEDIC IMPLANTATION APPLICATION

By: David Holomakoff

Thesis Advisor: Dr. Michael Mason

An Abstract of the Thesis Presented
in Partial Fulfilment of the Requirement for the
Degree of Master of Science
(in Biological Engineering)
August 2017

The field of biomaterials is of immense importance and will continue to grow and develop in the coming years. Novel materials, as well as new approaches for use of existing materials, are sought after now more than ever. Current metal orthopedic implants have an over engineered stiffness and Young's modulus, causing a phenomenon called stress shielding. Metal implants absorb the majority of force typically exerted on bone and the osteocytes within. When osteocytes fail to sense mechanical forces bones become less dense and weaken, causing possible fracture and other complications. A new orthopedic material is needed matching Young's modulus of bone (0.1-40GPa) and is tunable. This thesis investigates the use of dewatered cellulose nanofiber (CNF) based solid-forms for use in biomedical applications; specifically as synthetic bone and bone scaffolds. In this application, it is paramount that all materials be biocompatible, and if not biodegradable, resistant to long-term biological attacks *in vivo*.

The engineering task of dewatering the cellulose nanofiber slurry was solved via a combination of capillary action, convection, and lyophilization. This process produced CNF solids in a wide range of controlled and selected porosities. Three point bend testing suggested a

correlation between CNF porosity and Young's modulus. Further suggesting tunability of Young's modulus of CNF is possible. Results suggest porosity of CNF solids is an important feature that predetermines strength of the material and surface area for possible osteocyte growth. Low porosity CNF solids were found to have a maximum Young's modulus of 6GPa, Maximum stress yield of 80GPa, and maximum compressive and tensile stresses of 30MPa and 25MPa respectively. This is comparable or better to poly lactic acid, a state of the art orthopedic polymer, and collagen, the fibrous protein found in bone and other connective tissue. Viscoelastic properties of CNF with confirmed and found similar to bone. High porous CNF was found to be press moldable and low porous CNF highly mechinable. Orthopedic fixation plates and screws were fabricated via a lathe and CNC device, yielding positive qualitative results while mimicking the shape of the existing art.

DEDICATION

For my loving and supportive parents who have always been there for me every step of the way. Always leading by example and never losing faith in my abilities. I love you extremely and would not be the man I am today without you. Also to Robert Sarrazien 1991-2015. Rest in peace, my friend. I will prove you right.

ACKNOWLEDGEMENTS

First and foremost I would like to thank my Advisor, Dr. Michael Mason, for never losing faith in me if I struggled to find direction for such a new and unique thesis project. For being there to not only mentor me in work but in life. My friends Aileen and Aimee Co, without their continuous, support me graduating would not be possible. My friend Jeremy Grant, for always keeping me grounded and always being a close life mentor; for which I will never take for granted or forget. My parents, my family, and my loving girlfriend Tess for their endless support. Last but not least the Maine Cancer Foundation and the Forest Bioproducts Research Institute.

TABLE OF CONTENTS

LIST OF FIGURES

LIST OF TABLES

LIST OF ABBREVIATIONS

CNF- Cellulose Nanofibers

PCNF- Phosphorylated Cellulose Nanofibers

PLA- Poly Lactic Acid

PLLA- Poly-L-Lactide

PGA- Poly Glycolic Acid

SEM- Scanning Electron Microscopy

HA- Hydroxyapatite

TCP- Tri Calcium Phosphate

XPS- X-ray photoelectron spectroscopy

CHAPTER 1

INTRODUCTION

1.1. Review of Medical Implants and Biomaterials

In the field of biomaterials, when researching and developing a new material multiple factors have to be considered. Firstly, one must fully understand the purpose of the material and its function. Will the material require biodegradation or will it need to stay *in vivo* indefinitely? In the case of orthopedic biomaterials, biodegradation is not ideal in most cases. If the material is not biodegradable then it must withstand long-term biological attacks *in vivo*. This requires the material be non-corrosive and non-inflammatory or lacking an immune response. A material must be well established with these inert properties before it can be considered for orthopedic use. The materials purpose and function must be questioned again while considering the physical and mechanical properties required. Must the material be elastic, hard, or porous? Is there a desired flexural modulus, fracture strength, or fracture toughness?

The targeted functions will determine whether a metal, ceramic, polymer, or composite material is needed. Composite materials, made of two or more independent materials, allow mechanical compromises to be made that are ordinarily impossible for independent materials. This is the selection process that helps select a good biomaterial. However, even with this process, many materials selected are suboptimal for their application. Because of this the search for novel, more optimal materials is always underway.

The search for novel biomaterials arises in an industry saturated with metals. These metal alloys provide a list of benefits that have established them as staples in biomedical implantation: Superior strength, resistance to shear stresses, resistance to corrosion, and biocompatibility.[4, 5] However significant faults have arisen since the turn of the century to suggest many metal alloys

have cons that outweigh the pros. Long term wear and tear in joints of orthopedic metal implants release sub-micron particles into localized synovial fluid. These localized particles create phenomena such as aseptic loosening and periprosthetic osteolysis. The bone loss, or osteolysis, occurs as macrophages phagocytose wear created metal particles within the localized joint. These phagocytes then stimulate various cytokines such as IL-6, IL-1β, and TNF-α. All of which induce the activation of local osteoclasts that begin the process of bone resorption.[7] The process of dissolving the bone away causes the implant to become unstable and insecure, or aseptic loosening.

Metal Alloy orthopedics induce bone resorption via additional factors; compounding into even greater risk. Stress shielding, a mechanical effect occurring in structures combining stiff materials with those that are more flexible, is responsible for this additional bone loss. The stiffness of the material is measured by Young's modulus, or the force required for the material to bend. The Young's Modulus of metal implants are 116 GPa for titanium alloys, 190 GPa for stainless steel, and 210-250 GPa for various cobalt-chromium alloys. Inherently human bone is significantly

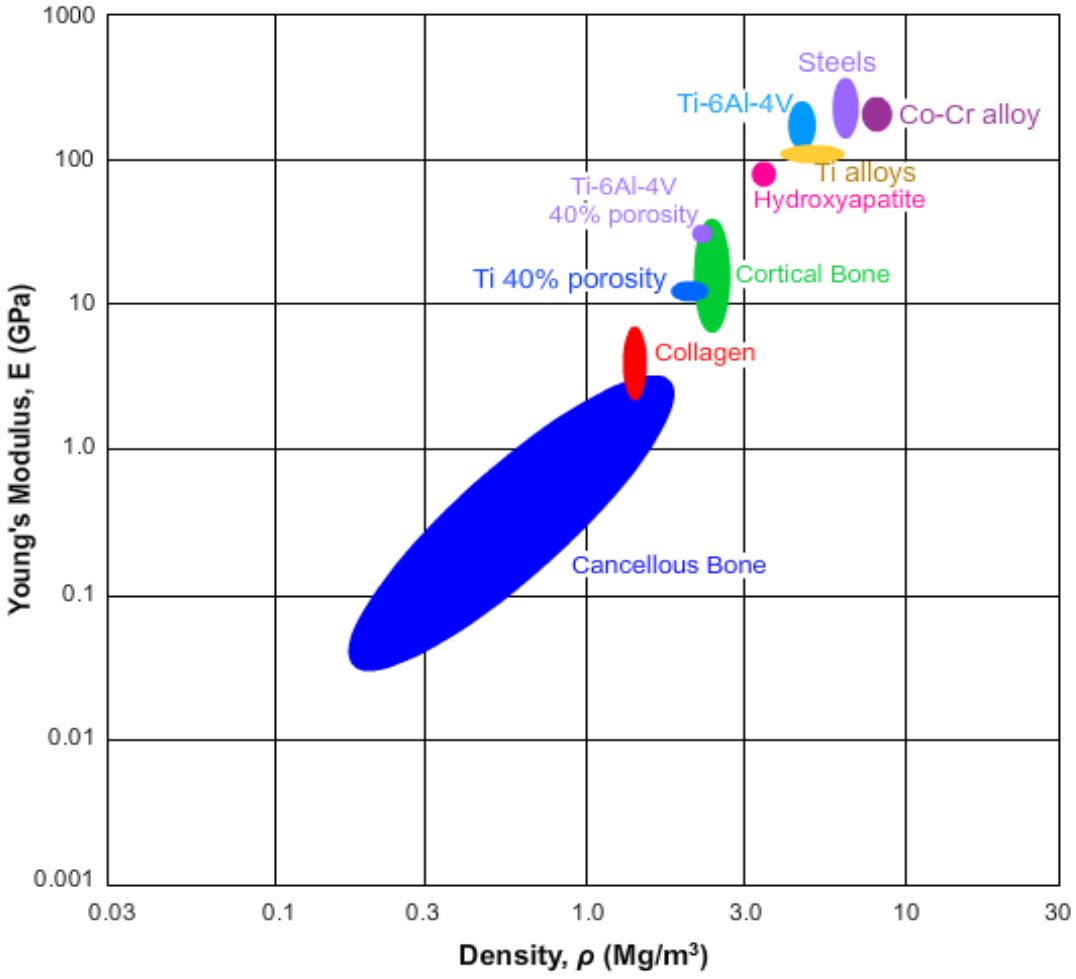

Figure 1.1 Graphical representation of Young's modulus vs. density of metal alloys that make up modern orthopedic implants and the materials that make up the composition of bone.

more flexible; with a Young's modulus of 1-20 GPa for high porosity low strain bone and 40 GPa for the less porous, high strain bone.[8] A graphical representation of this can be found in Figure 1.1. It is observed the only metal-based material produced with a flexural modulus and density similar to cortical bone is 40% porosity titanium. This is a logical step mechanically. For most materials, the simplest way to manipulate the Young's modulus of a material is to change its density/porosity. Cancellous bone has a wider span of flexural moduli because of its porous nature and a wide range

of densities. Suggesting an optimal analog material for bone should possess a density that can be manipulated with ease. The porous titanium technology incorporates a high-powered laser to melt and shape titanium powder into solid forms. This incorporates solid freeform fabrication (SFF) to achieve Laser Engineered Net Shaping (LENS™) of a Ti6A4V alloy powder as illustrated in Figure 1.2.

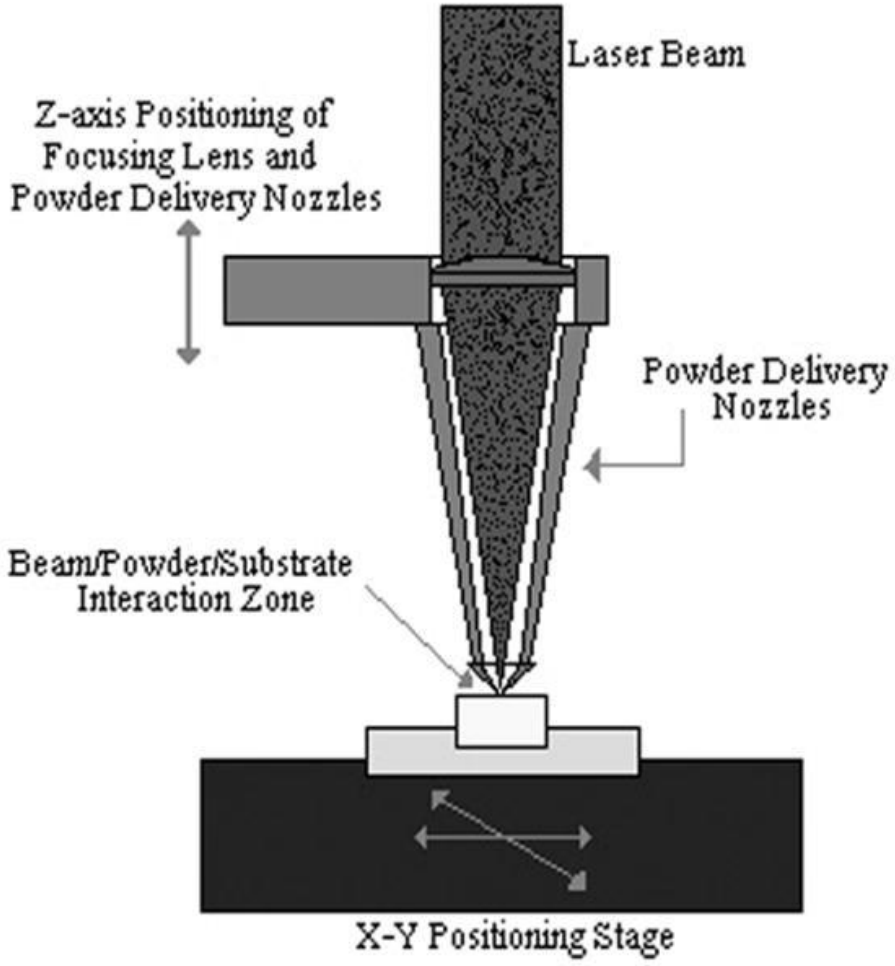

Figure 1.2 A schematic representation of the LENS™ process. (Ref 9)

This process has multiple advantages over conventional powdered sintering for producing porous metals. Not only is the pore size and shape in powdered sintering unable to be controlled, but sintered metals are more likely to obtain stress induced cracks and are extremely brittle in

comparison. The instrument is capable of creating titanium alloy with pore volume fractions ranging from 19-40% porosity. This pore range is visually represented in Figure 1.3 in the form of titanium cylinders. These porosities are capable of Young's moduli ranging from

7-60GPa. These results mimic the range of flexural moduli capable from human bone; a large breakthrough in prosthetic technology. Unfortunately for the current technology, tuning of Young's modulus still requires improvement. A strong correlation between porosity and Young's modulus has not been proven.[9] Porous titanium is a step in the correct direction. More research and development is needed with these materials. However the material platform with be limited going forward as it is metal and non-organic.

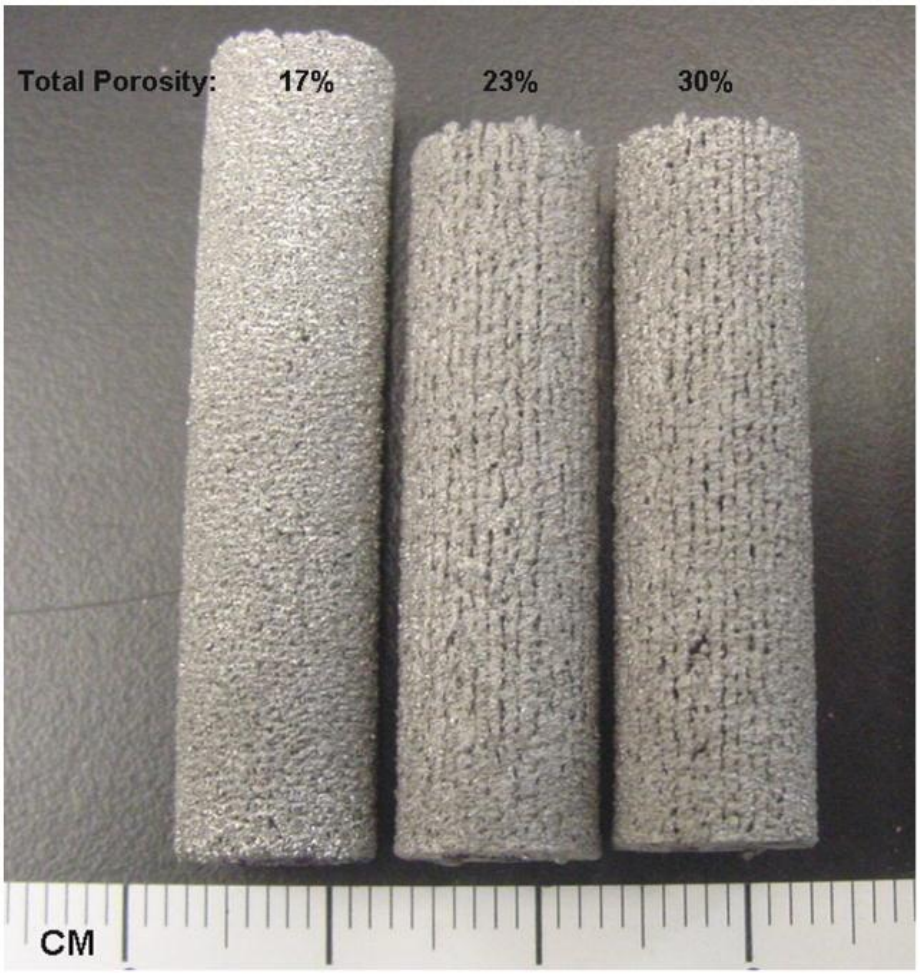

Figure 1.3 Porous cylinders of titanium produced through the LENS™ process at varying porosities. The structure, size, and shape of the pores are controlled through a three-dimensional image produced in CAD. (Ref 9)

As stated previously, with the stiffer material introduced more stress and strain is shielded away from the more flexible bone. Observing this active phenomenon we refer to Wolff's law which states: The reduction of bone stresses in contrast to a typical stress environment will cause the bone to adapt and reduce its density during the process of resorption around the implant. Bone contains valuable minerals such that if cell signaling dictates minerals are used improperly; resources will be correctly redistributed from the unused bone. With less mineral density bones are more likely to break and fracture. This causes a complete failure of the implant, requiring

immediate surgery. A second surgery can cause further complications to the joint and may not be a viable option for elderly patients. Bone resorption is a serious condition that requires a reduction in its frequency and eventual elimination. The condition is purely a side effect of current ignorance to a solution.

A solution requires an orthopedic material to have the same flexural modulus and density as human bone. In addition, this material must meet all the standard criteria of a long term biomaterial. It must be non-corrosive, non-inflammatory and inert to an autoimmune response. Because bone is a composite material made up of collagen and hydroxyapatite; it is possible a perfect bone analog may be a composite material as well. Requiring both an elastic material and a brittle material of significant toughness and hardness.

1.2. Review of Cellulose Nanofiber and the Known Properties

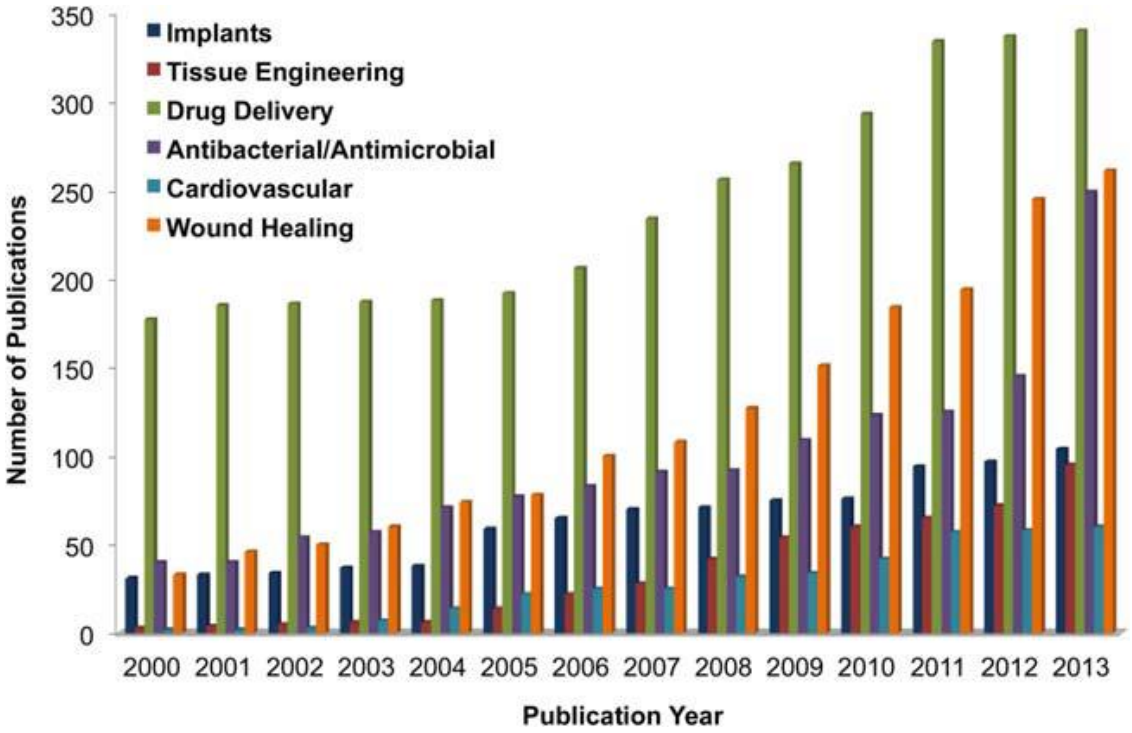

Figure 1.4 Representation of the annual increase of Nanocellulose publications in the biomedical field from the years 2000-2013. (Ref 10)

The field of biomaterials is of immense importance and will continue to grow and develop in the coming years. Novel materials, as well as new approaches for use of existing materials, are vigorously sought after. Figure 1.5 identifies this trend. Within the orthopedic field, this is no different. Nanocellulose is among the more novel, unique materials that have been subject to research and development.

Independent of the unique physical properties; nanocellulose is derived from the cellulose polymer, the most abundant polymer on the planet. Cellulose has an estimated Bioproduction rate of $7.5 * 10^{10}$ metric tons every year.[1] Sourced from wood, cotton, hemp, flax, wheat straw, sugar beet, potato tuber, algae, etc. The future ensures this supply of cellulose. Contrary to other materials cellulose nanofibers have proven to be bio-inert; producing an extremely limited

inflammatory response *in vivo*.[2, 3] Represented in Figure 1.4, cellulose polymer accrues its strength through hydrogen bonding between the chains of ***β***(1,4)-Linked D-glucose units. Cellulose nanofibers have advantages over traditional cellulose because of decreased fiber size. Decreased fiber size creates a greater over all surface area within the fibrous matrix.

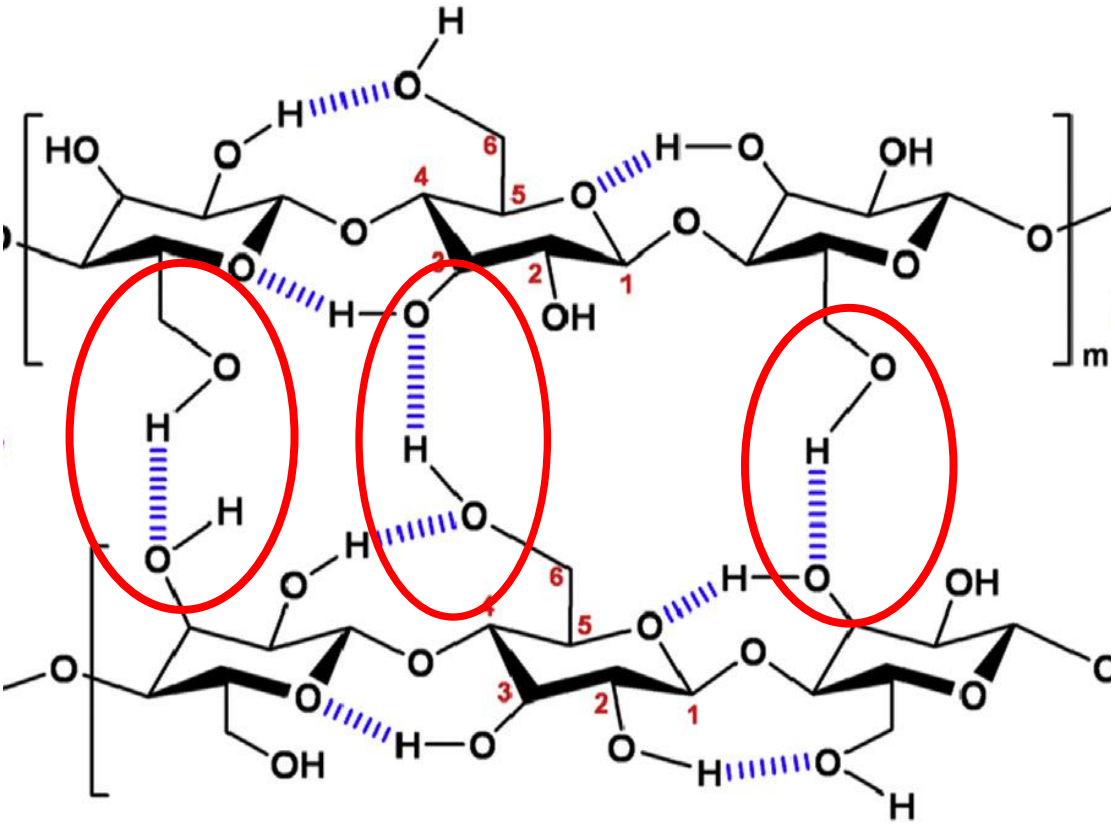

Figure 1.5 The hydrogen bonds that link together the cellulose polymer chains; inherently giving cellulose strength.

This larger surface area allows for greater hydrogen bonding to occur and therefor create a stronger material. Nanocellulose fiber garners its name from the fiber diameter. Fiber diameters are on the nanoscale, ranging from 50-250nm.

Nanocellulose itself comes in three different forms; two variants of fibers and one variant of the crystalline from. The crystalline form, or cellulose nanocrystals (CNC), have unique and sought after properties in the biomedical field. These properties, however, have less viable

application in the areas of orthopedic and structural implants. The fibrous forms of nanocellulose are more promising in this regard. Bacterial nanocellulose (BC) are cellulose nano fibers that have been produced and built in a structured matrix by living prokaryotic organisms. These matrices are typically of small volume and mass. This factor may potentially limit certain large scale application. BC is the least cytotoxic of all nanocellulose types; showing no levels of toxicity of any kind.[21 25 26] Because of this reputation, BC has been a popular selection in many biomedical studies where soft tissue is involved. Despite various advantages, it is assumed BC is a non-optimal choice when considering alternative materials for large scale orthopedic implantations. Mechanical properties of the BC are more similar to soft cartilage than to human bone.[18] Large scale production of BC is additionally limited by the metabolic processes of your bacteria. Currently, the fasted production of BC is 0.38 g/(L h) using an aerosol bioreactor.[26] These are insignificant quantities to produces orthopedic devices on an efficient scale.

While the biosynthesis of BC is a mechanism of construction from some of the smallest units (A), up to units on the nanoscale (nm); the production of cellulose nanofibers (CNF) is exactly the opposite. Typically a mechanical or chemical process is preformed that strips down larger, microscale cellulosic fibers, down to fibers on the nanoscale. CNF is more commonly created in an industrial setting contrary to a laboratory setting. It is capable of being produced in large quantities; with smaller batch operations capable of creating two tons per day. Inherently making CNF an optimal choice for biomedical processes requiring large volumes, and ideal for orthopedic implantation which requires large volumes of biomaterial. The most common physical form of CNF is an aqueous matrix that has the ability to flow at approximately 3 wt.% fibers. When dehydrated, CNF has a similar microscale fibrous matrix to BC. Differences arise when fiber orientation is examined. BC maintains a more organized webbing as it is created by

microorganisms. The hydrogen bonding of the CNF is energy dependent making fiber orientation affected by a wide variety of factors.

Cellulose nanofibers have proven a viable biomaterial in various applications. Current research resides in fields such as wound healing, cardiovascular, drug delivery, antibacterial, tissue engineering, and implants. Publications in all fields mentioned are increasing annually in frequency. A potential biomaterial must undergo extensive cytotoxicity and biocompatibility testing. CNF cytotoxicity testing was performed on both human monocytes and mouse macrophages. The study resulted with no observed cytotoxicity of the cells and with no inflammation response occurring at time points of 6 and 24h.[11] In vitro testing for CNF genotoxicity has been performed with an enzyme comet assay. It was concluded that no significant DNA damage was shown.[12] The effect of cellulose nanofibers on neurons and neurotoxicity are well documented. Neurotoxicity and systematic effects using both in vitro, and nematode *in vivo* model were measured at low levels or failed to be detected. Only marginal effects were seen at the maximum doses of 2mg/ml. It was concluded the likely cause was the mechanical intrusion of cell movement and cell signaling. The same study found only slight damage to occur in bronchial epithelial cells in vitro. These results are identical to a number of nanomaterials that are typically considered "inert."[13] [14]

Further testing on mammalian cells has included cell membrane stability, cell mitochondrial activity, and DNA proliferation in the presence of CNF. These examinations were run on pure, unmodified CNF with 3T3 mammalian fibroblast cells. Cell membrane, cell mitochondrial activity, and the DNA proliferation remained unchanged during the tests. This remained true for both direct, and indirect contact. CNF modified with CTAB and PEI on the surface revealed some levels of cytotoxic effects.[15] It is then suggested these modifications should

not be used when a biological application is desired. Trimethylammonium (EPTMAC) treated cellulose nanofibers induces increased ingrowth of human epithelial cells and created a more cytocompatible profile than non-treated CNF.[17] Pure CNF disrupts cell function and signaling at significant concentrations. Cell apoptosis associated X-protein is expressed at 2000 and 5000µg per milliliter; along with heat shock proteins HSP70.1 and PRDX1.[16]

Because of the proven biocompatibility of nanocellulose, research has started within the biomedical field to examine its application as an implanted analog material. In recent years there has been increased interest in the development of Nanocellulose based materials for soft tissue replacement and tissue reconstructive applications. This is increasingly true with the form BC. Mechanical properties of bacterial Nanocellulose gels have been compared with the collagen constructed meniscus implants and menisci from pigs. The Nanocellulose was found to be significantly stronger than the collagen implant, and not as strong as the real pig meniscus. It was reasoned that the ordered structure of the collagen within the real meniscus led to superior strength.[18] The combination of cheap material cost, simple growth shape manipulation, and promising mechanical strength indicate cellulose nanofibers as a favorable option for a collagen and soft tissue analog material.

The similarities bacterial nanocellulose has to collagen have induced further studies into cartilage replacements. BC was grown into the shape of a human ear using a negative ear mold created by an MRI scan. The mold growth was successful and implies that each ear may be custom cast from patient to patient. Mechanical examination suggested that at an effective cellulose content of 14% matched the instantaneous modulus, equilibrium modulus, and maximum stress yield of cartilage taken from four human ears.[19] To further test the limits of bacterial nanocellulose; the friction factor and wear behavior of the material was characterized under simulated biological

conditions. This characterization was performed against bovine articular cartilage hydrated by PBS solution. Under a steady state friction regimen using pin-on-flat wear testing; BC executed notable resistance to wear. This was credited to the compact nanostructure of the mechanically resistant nanofibers. The physical wear of BC was characterized as plastic deformation via displacement of thin layers of material.[20] This conclusion is understandable as plastic deformation is typical in polymer structures.

The cellulose nanofibers produced at The University of Maine are created in a Masuko MKZB15-50J super mass colloider. This colloider uses two ceramic non-porous grinding disks to created large shear rates; tearing down the lignocellulose fibers that are input into the hopper of the machine. The output product is a white paste made up of 3wt% cellulose nanofibers and 97% water. In this form, Nanocelluose has very limited biomedical application. Difficulties with this material form occur because of the same hydrogen bonding that makes this material intriguing and of high interest. The hydrogen bonding creates an extremely hydrophilic fibrous matrix in paste form. To create a solid form material all the water must be removed from the matrix. There are multiple constraints to consider when manipulating this material with the intention of creating solid forms of significant volume. Hydrogen bonding from the cellulose polymer creates a fully hydrophilic and hygroscopic environment. This physical phenomenon must be overcome before the cellulose nanofibers are in a machinable form.

1.3. Machined Nanocellulose Plastics for Biomedical Implantation

As there are multiple and widespread issues regarding medical large scale orthopedic replacements; problems exist within similar veins regarding the orthopedics of bone fixation surgeries. Currently, two material platforms control the market of orthopedic fixation devices; titanium alloys and synthetic hydroxyester polymer composites. Each material platform

representing a different chapter in the industry of biomedical materials applied orthopedics. Titanium alloys emerged as the optimal metal for medical use after 50 years of trial and success, proving more successful than cobalt-chromium and stainless steel. However, the technology behind this material platform has grown long in the tooth. Synthetic hydroxyester fixation devices were engineered in response to reported shortcomings with titanium fixation. Examples of these synthetic polymers include Poly-lactic acid (PLA), poly-L-lactide (PLLA), and poly-glycolic acid (PGA). These polymers are capable of complete dissolution into the human body and therefore

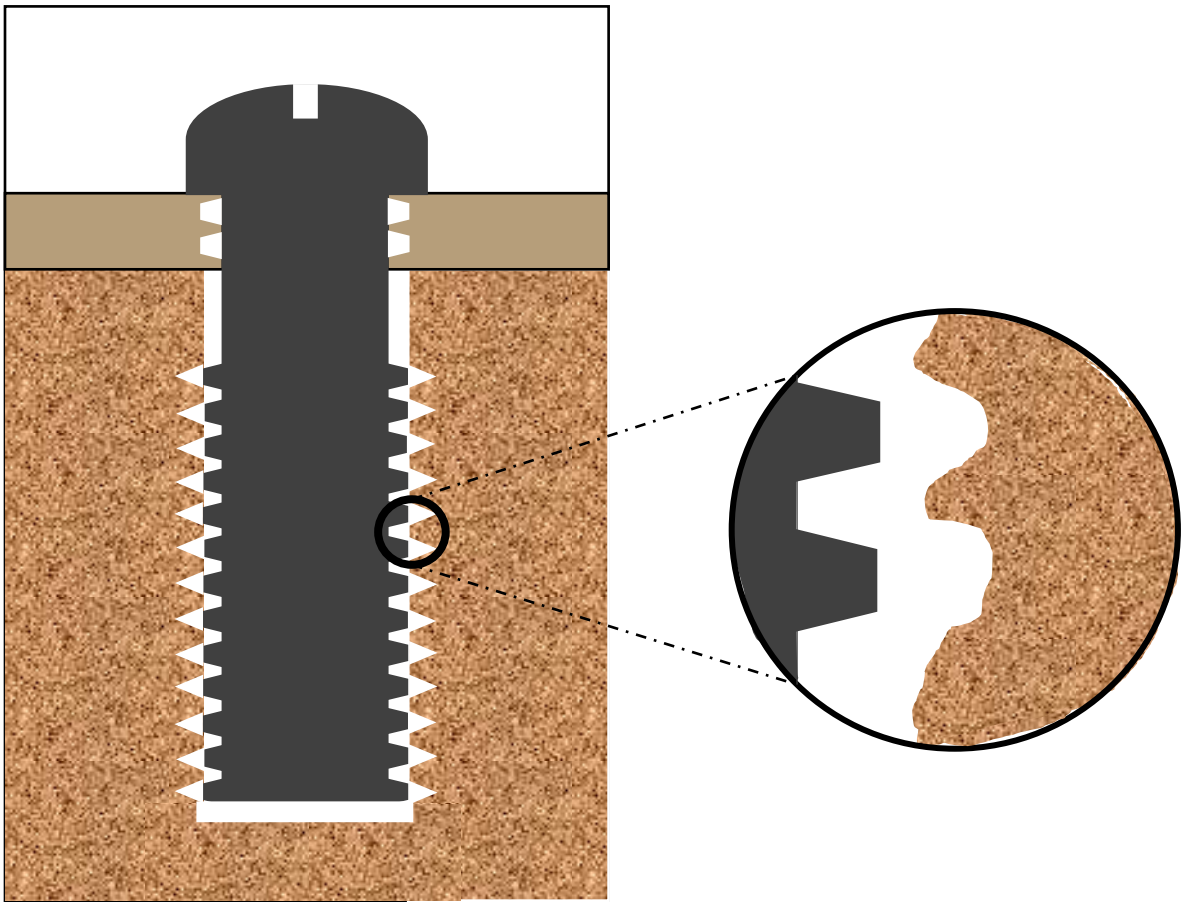

Figure 1.6 Aseptic loosening cartoon of a titanium fixation screw. Bone degeneration at the screw-cancellous interface can be observed. This pocket of extracellular fluid allows screw movement that exceeds the tolerance of the design. This movement can cause stress fractures and further inflammation to the patient.

lack the need for surgical removal. The supplementation of hydroxyapatite (HA) and Tri calcium phosphate (TCP) into hydroxyesters allows for further material applications and allows osteocyte ingrowth as the material dissolves.[22] Unfortunately these synthetic polymers similarly possess design flaws for biological systems.

As with orthopedic joint replacements, titanium fixation devices such as screws, plates, and pins, suffer from the biological constraints the material possess. The overbearing Young's Modulus and strength of the titanium chronically cause stress shielding around any boney tissue the titanium occupies. Wolff's law still applies to the biological system despite material shape or mass of material. With osteolysis occurring around the fixation screw or plate, small pockets of extracellular fluid can appear as the osteocytes pull away from the titanium. This process is represented in Figure 1.6. These pockets can create micromotion when force is applied; the first steps to aseptic loosening of a device. [21] Previously stated, aseptic loosening not only causes pain and discomfort; but can lead to a secondary surgery for the patient. Inherently, a second surgery is costly, time consuming, uncomfortable, and potential health threatening. In addition, the removal of titanium pins and screws from bone tissue result in empty chasms within the bone. These void spaces will most likely not fill in; creating mechanical weak points within the bone. Weak points can potential cause bone fracturing, causing further pain and further complications.

In response to the numerous shortcomings with titanium based devices, polymer technology for medical application was highly researched. The result of this are the group of synthetic polymers PLA, PLLA, and PGA; all of which are hydroxyesters. The major advantage of these polymers is they are biodegradable, allowing them to dissolve *in vivo* and eventually completely clear the boney tissue. These polymers also avoid stress shielding characteristics, collectively having a Young's modulus range of 2-6GPa as raw materials.[22] While these are

passible Young's modulus values for bone and connective tissue, mimicking that of spongey bone and collagen; yet lacking the strength necessary to replace the mechanics or dense cortical bone. To combat this mechanical disadvantage, hydroxyapatite and Tri-calcium phosphate are added to the material as it is sintered and molded. Not only do these minerals add mechanical strength and integrity to the newly formed composite, but also provide a new mechanic of osteocyte ingrowth as the polymer dissolves away. The dissolving polymer provides new space within the material matrix for bone cells to flow within, the mineral provides a biological site for the cells to grow and produce new bone tissue.[23]

These synergistic effects appear advantageous, however, this material has multiple disadvantages that prevent an all-encompassing solution. Because the single units of these polymers, lactic acid, and glycolic acid, are acidic in nature, as these polymers dissolve *in vivo* localized acidification occurs. Acidification leads to complications with local osteocytes and boney tissue. Increased acidity creates bone degradation in the localized area around the fixation device. This bone degradation decreases bone ingrowth and causes aseptic loosening of the fixation units. The solution to bone fixation materials is a one that is biodegradable, allows bone ingrowth, lacks acidification, lacks an immune response, and maintains proper mechanical properties to withstand biomechanical stress. This will most likely be in the form of a polymer or polymer-mineral composite. Nanocellulose is a polymer with non-acidic biodegradation capabilities that possesses interesting characteristics that require further study. This will be the main focus of this project.

CHAPTER 2

DEWATERING OF NANOCELLULOSE FIBERS

2.1. Introduction

Aforementioned, a significant number of engineering challenges arise went attempting to efficiently remove water from slurries of Nanocellulose fiber. Hydrogen bonding between water molecules and the cellulose polymer create a hydrophilic environment which requires input energy to overcome. This can be identified as the main challenge the material present. The physical form of the material (3wt% slurry) is an additional challenge that presents itself. There are two physical characteristics that induce this challenge. The viscosity of the CNF produced from the Masuko Super mass colloider will flow under physical manipulation due to low viscosity. The CNF viscosity creates the need for a mold or container to hold the material as it dries into a more solidified unit.

The fibrous slurry is 97% water by weight, and 95.6% water by volume. Causing the volume of the matrix to theoretically decrease by 95.6% when drying the CNF to completion, or maximum density ($1.5 g/cm^3$). A volume decrease of high magnitude will create challenges when forming a material into a desired size or shape via mold. Determining a model for calculating the product mold with detailed features would become an intensive endeavor. A simple alternative is to dry CNF into uniform solid bricks, or ingots, which will be machined into a desired form. Calculating the final mass and dimensions of CNF ingots is significantly more trivial when compared to doing the same with complex structures. Ease of reproducibility is paramount when producing material for orthopedic implants. The suggested drying strategy must not only dry the CNF material to completion but create dry CNF matrices of a wide range of densities and porosities. Freeze drying is a standard practice to remove water from a material while maintaining

its current volume and shape. In the case of CNF, removed water will act as void space within the dry fibrous matrix. The less water, the denser the CNF matrix will be after freeze drying. If a controlled method of water removal is created; freeze drying may lead to production of CNF material with a controlled, predictable porosity.

Typical CNF production at The University of Maine results in the packaging of 5 gallon buckets. Because of the theoretical volume decrease of 95.6% from bucket to dense product, it is determined drying a single 5 gallon to completion will make an ideal small scale batch; producing a CNF brick of approximately 832.93cm^3 in volume. This volume should be sufficient for machine testing and manipulation of material for mechanical testing and material characterization. It is now determined a drying mold must be constructed that meets the following parameters: The mold must hold the contents of a 5 gallon CNF bucket, the mold must effectively dry the material that it contains, it must maintain the ratio based dimensions of a typical rectangular block or brick. A 3:1 length to width ratio would be sufficient. When one assumes a 3:1 ratio and a 5 gallon volume, a 5" width, 15" length dimension appear as an efficient inner footprint for a mold of tolerable small scale height (16").

2.2. Methods

2.2.1. Capillary Action

Capillary action is a physical phenomenon created by a combination of adhesion and cohesion forces of a liquid, typically water. Cohesion, the attractive forces between the fluid molecules and themselves, and adhesion, the attractive forces between the liquid molecules and the surface of the capillary, have the capacity to propel a fluid in a desired direction without any outside force acting upon it. This manipulation of intermolecular forces can be seen as free energy,

as the system of moving fluid is self-sustaining. Common items such as paper towels and sponges use capillary action to displace water away from undesired areas. These items do so because of small pores the materials contain. This capillary process with porous materials such as paper is commonly titled “wicking” in industry. Sponges and towels are efficient wickers, but will most likely suffer in any large scale production where vast amounts of CNF must be dried repeatedly. Additionally, they will be unable to consistently withstand heating if thermal energy is added to the system.

Alternatively, there are many durable materials that maintain porosities viable for large amounts of capillary action and water displacement. Plaster and ceramics are cheap, common place, and possess large relative porosities that offer efficient wicking. Small scale experiments using ceramic cylinders were extremely successful in driving water out of the CNF slurry and allowing the fibers to bind together to a solid matrix. Despite this success with ceramic, plaster was chosen as simpler logistic alternative. Ceramics commonly must be cured in a large kiln or furnace, resources that were not currently available. Plaster can be cured at room temperature, creating a large advantage. Plans for the plaster mold were drawn. The thickness of the mold walls would be 1.5 inches, with an inner footprint of 15”x5”, and an outer footprint of 16.5”x6.5”. Plaster of paris (calcium sulfate dehydrate) was selected as a readily available plaster. A plywood shell was constructed and plaster of paris was mixed with water as instructions indicated. The mixed plaster was poured into the mold and left a week to cure.

Despite multiple methods used to prevent binding of the plaster to the plywood such as plastic wrap and Vaseline, there were difficulties removing the plaster without slight cracking of the mold. This is very likely due to low surface area of the air-plaster interface; it was observed that the plaster mold wicked inherently slowing curing of the material to a significant degree. The

plaster was left out to cure for an additional 24 hours. After the plaster appeared dry a five gallon bucket of cellulose nanofibers was poured into the mold top. The cellulose was to be dried within

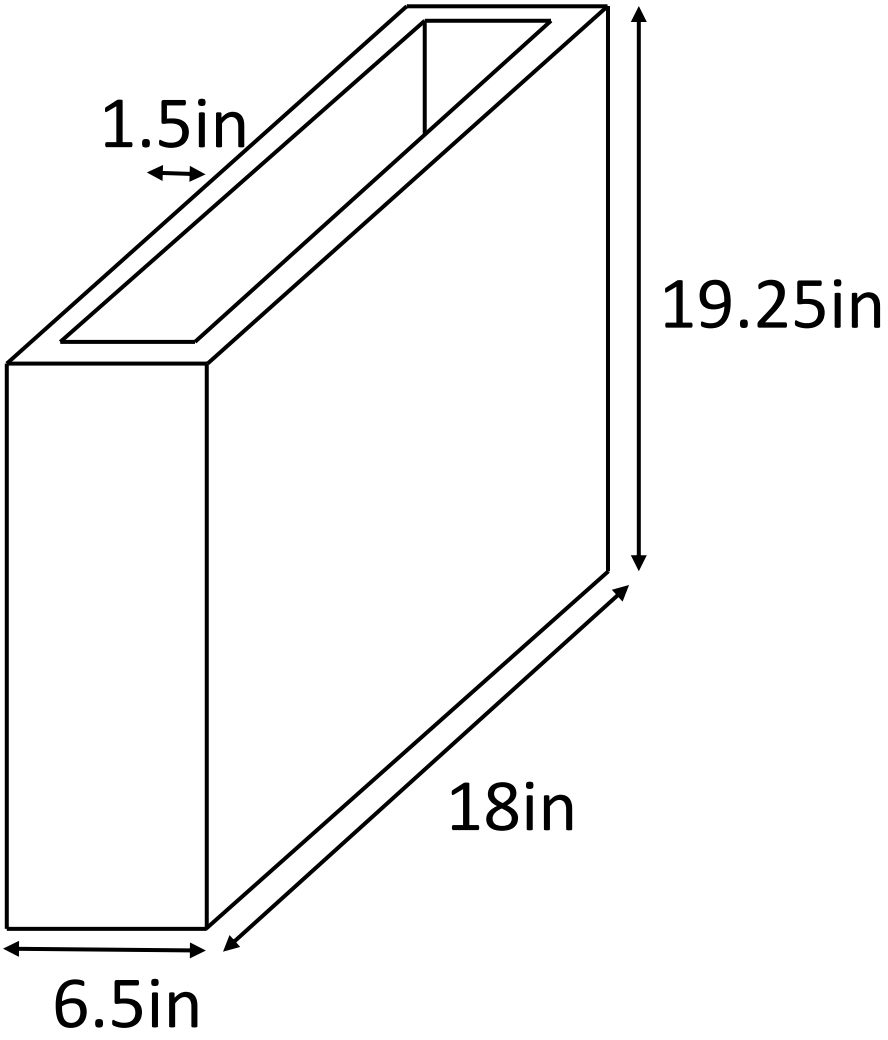

Figure 2.1 Planned dimensions of the dewatering mold for CNF. The mold was planned to be made out of plaster, however, this shape can be formed using a wide variety of materials. The main goal is the rectangular shape needed to form squared, mechinable ingots

the mold at ambient conditions. Water away from the CNF slurry via capillary action. However, when the plaster rehydrated and softened, it became structurally unsound. A hole was blown out in the side of the mold due to the hydrostatic pressure created by the 5 gallons of CNF.

In summary, the drying experiment was a failure. After the remaining plaster dried an additional week after the experiment, it was determined the plaster could have been mixed incorrectly. The plaster cured with a chalk type constancy and would leave a powder residue. This is abnormal for plaster of paris. It is likely that an issue with the mixing or curing procedure occurred. The plaster method proved to be time intensive and brought no results. It was decided alternative methods should be explored for an industrial capillary material.

Refractory brick, or fire brick, is a brick typically made of specific ceramic. It is designed to withstand high temperatures of a kiln, furnace, or fireplace. The difficulties of firebrick are well known within the mason industry while constructing fire places for chimneys. Firebrick porosity cause large capillary forces within the material. These capillary forces withdraw water out of the mortar that holds the firebricks together for chimney construction. When water is drawn out of the mortar it can no longer cure correctly. With improper curing, the bonds are weakened and the chimney becomes unstable. Because of this, masons will regularly submerge fire brick in buckets of water and let the pores saturate before mortar is applied. This evidence suggests fire brick should be further explored as a capillary material for CNF drying.

Further research identified sorptivity is an important measure of a material's capacity to absorb or desorb fluid. Sorptivity is measured with the units of length*time$^{1/2}$. The documented sorptivity of clay brick, a substance similar to fire brick, measures 1.16mm*min$^{1/2}$. Significantly greater than the porosity of concrete brick (0.2mm*min$^{1/2}$), another considered material. Plaster is measured to have a sorptivity of 3.5mm*min$^{1/2}$, over double the sorptivity of clay brick. However, one must consider two things while comparing the sorptivity of plaster and clay brick. Firstly, one must recall the failed experiment mentioned previous. Using a material such as fire brick would be a much simpler method in the short term. Secondly, the sorptivity of clay brick

that is published and the sorptivity of fire brick may not be identical. There are a large number of clay varieties, all with different porosities and mineral contents. It is likely the sorptivity differs from clay to clay. The qualitative observations of the firebrick material are impressive. It was then decided fire bricks should be purchased and their specific sorptivity tested in house.

Fire bricks were purchased measuring 9 x 4.5 x 1.25in dimension, half the depth of traditional firebrick. Reduced depth creates a shorter distance between the cellulose-brick interface and the brick-air interface; therefore having a shorter distance the water travels before it evaporates to atmosphere. Tortuosity is a term describing pore shape and continuity. A pore that is perfectly straight with no obstructions, has a tortuosity of 0. Where a windy, misguided, inconsistent pore will likely have a high tortuosity. It has been hypothesized the length the water travels will be one of the most important variables control. To prove these mechanics we reference Washburn's Equation, which describes capillary flow within a collection of parallel cylindrical tubes having minimal tortuosity. Wet-out flow is described as:

$$L^2 = \frac{\gamma D t}{4\eta} \rightarrow t = \frac{4L^2\eta}{\gamma D}$$

Equation 2.0 Washburn Wet-out flow. Original and rearranged to show in terms of time.

L= Capillary Length

γ= Surface Tension of Fluid

D= Pore Diameter

η= Dynamic Viscosity of Fluid

t= Time

Mathematically, this system can be modeled an alternative way using similar principles. The water removal via capillary action is physically dependent the pressure change the capillary creates across the interface between the two static fluids. In this case, the two fluids are water and air. It is this change that withdraws the water out of the CNF and into the firebrick. The capillary pressure is defined by various characteristics of the pore, such as size and tortuosity of the capillary; and the wettability and thickness of the mold material being applied. Empirically this capillary pressure is modeled by the Young-Laplace equation:

$$\Delta P = \frac{2\gamma cos\theta}{r}$$

Equation 2.1 Young-Laplace equation for capillary pressure.

ΔP= Capillary Pressure Differential

γ= Surface Tension

θ= Contact Angle

r= Capillary Radius

When applying this calculation to a highly wetting surface, it can be assumed the cosθ≈1. After this assumption, the capillary rise approximation can be applied to the capillary pressure difference. This can be seen below:

$$\Delta P \approx \frac{2\gamma}{r} = \rho g h$$

Equation 2.2 When cosθ≈1 is assumed, capillary pressure can be set equal to the capillary rise approximation.

From the above equation, additional modifications can be made to better represent the current physical system. Because the water is being wicked horizontally, the term for height (h) can be substituted for width (w). Because the capillary system is assumed to have minimal tortuosity, a horizontal system lacks the need for gravitational force (g). A non-tortuous system will never change position in the Z-axis. Using these assumptions Equation 2.2 can be rearranged to solve for width, or width max, of the porous material:

$$w_{max} = \frac{2\gamma}{\rho r}$$

Equation 2.3 Maximum width of porous material needed to properly clear water out of CNF and through the pores to the outside air interface.

Equation 2.3 is an idealized model that not only requires straight, cylindrical pores with minimal tortuosity but additionally requires a uniform pore size throughout the wicking material. Because uniform pore sizes are unnatural in many materials, the w_{max} calculated will likely be a width range rather than a single value. Furthermore, because of the tortuosity assumption, this expression will calculate widths larger than needed for real life material applications.

Figure 2.2 Iron welded frames used to hold the capillary material (fire brick) in place, creating a drying mold for the CNF aqueous slurry. The frames are designed so that bricks can be slid into place to make a tight seal; preventing loss of any fiber.

It is observed that the length term in the wet-out flow equation is the greatest contributor to time as it is to the second power. Because the dynamic viscosity and surface tension of water within the cellulose nanofibers cannot be manipulated, the distance of the capillaries is the most important variable to control within the system. A simple empirical model has been generated to assist in selecting this length (L) in non-tortuous systems. It was planned to orient the fire brick

in similar dimensions as the attempted plaster molding; capable of holding 5 gallons of 3% CNF slurry in a rectangular chamber. Angle iron frames were welded into skeletal forms to support the fire brick. This can be seen in Figure 2.2, both empty and loaded with brick.

The frame is sized so bricks may be slid in and out with ease. The specific orientation chosen may also be observed in Figure 2.2. Simple addition and removal of the firebrick is of paramount importance to ease access to the CNF within the fire brick mold. This replacement process creates easy plug and play capabilities to replace bricks that have pores that are clogged or currently hydrated with water. When fully assembled, the drying apparatus (frame and bricks) has a mass of 100lbs and is not easily mobile. The apparatus has a small footprint of 7.5in x 17.5in. Small enough to fit a large quantity into walk-in ovens for high throughput.

2.2.2. Convection

Adding thermal energy to any system is a viable and popular method of water removal. A common example of thermal energy in this application are convection ovens, ovens implementing fans or other means to circulate hot air around the sample being heated. A vented convection oven typically further assists the process of drying hydrated samples. Removing humid air from the oven will maintain a larger humidity gradient; increasing mass transfer properties of the water vapor leaving hot CNF. After capillary action pulls water from the CNF and perspires it from the outside of the brick, this vaporization of the outside face is the most important step to removing water from the system. In addition, when enough water is removed from the CNF matrix the volume of the material will greatly decrease. This causes the CNF matrix to pull away from the fire brick, disengaging capillary action from further occurring on the four walls of the CNF ingot. The four walls then become a CNF matrix-air interface; increasing the importance of thermal convection as it becomes the sole driving force for dehydration within the system.

2.2.3. Lyophilization

One material advantage of cellulose nanofibers is the capability of porosity control. Lyophilization, or freeze drying, is the key mechanism to this control. Freeze drying uses a vacuum pump to create a vacuum of approximately 30mTorr to sublimate water vapor off a frozen sample. Freeze drying creates the capability to permanently lock the fibrous matrix in a current orientation at any given time. The ice is removed from the frozen sample leaving void space, or porosity, within the sample. For example, a sample of 20% cellulose and 80% water will be lyophilized to a CNF solid of 80% porosity. However, because the 9% volume of water changes during the phase change to ice, this volume change must be modeled. This modeling is represented in Figure 2.3; for both frozen and non-frozen samples. When the results are observed it is noted both curves are extremely similar. Despite the 9% volume increase from water to ice, the overall mass fraction, or percentage, of cellulose nanofibers within the matrix changes very little in comparison.

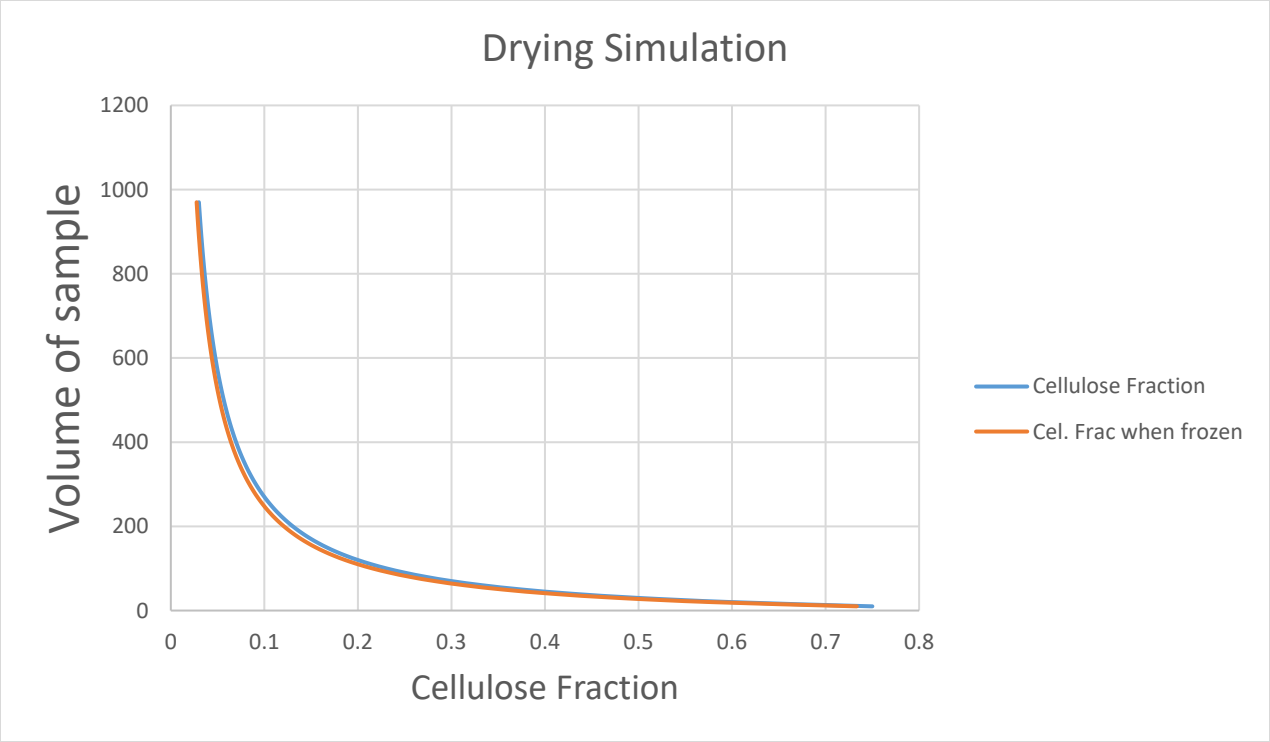

Figure 2.3 Modeling the cellulose fraction change as volume of the sample decreases. This includes frozen samples and non-frozen samples. It can be observed the cellulose fraction are very similar for both sample types.

In addition, it is observed the maximum difference from frozen to non-frozen occurs at the mass fraction of 0.1(10%). This is the regime where the volume of water phase changing to ice contributes the most to the overall volume change of the sample. It is noted the difference disappears as the cellulose volume fraction becomes larger than the water fraction. This information is important to correlate water volume % before freezing drying to porosity % after freeze drying. When running experiments it can be safely assumed water volume% before freeze drying will approximately equate to porosity%; with a maximum modeled uncertainty of 5.9% at

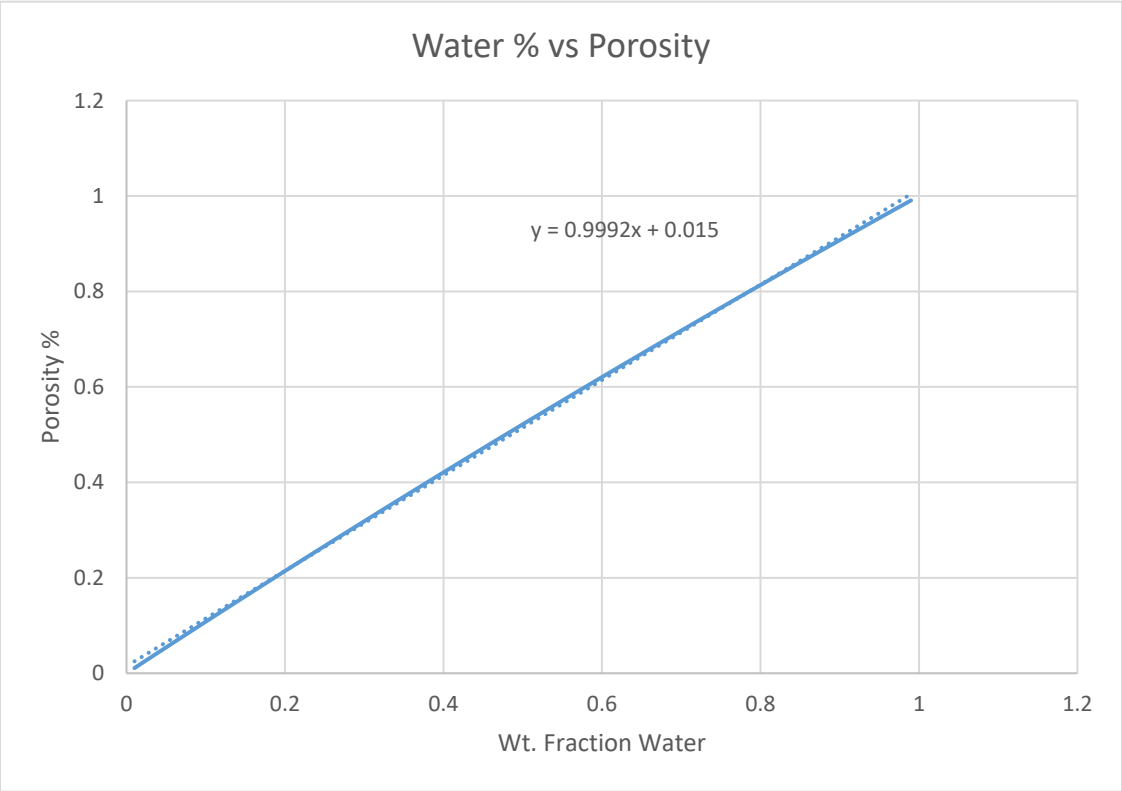

Figure 2.4 Correlation function of Water Volume% to Porosity% of the CNF solid after freeze drying

a 0.1 cellulose fraction. This correlation is modeled on Figure 2.4. It is acknowledged this function is solely a model and is free of real world, experimental uncertainty. Because of this, it is acknowledged the assumed correlation will not be as accurate as the model represents.

The procedure for lyophilizing CNF is as follows. During drying within the firebrick mold, a desired wt. % of nanocellulose fiber was selected and removed from the drying CNF matrix. If a shape was required of the cellulose nanofibers it was shaped via compressive force and placed within a lyophilizer jar, a Pyrex jar designed to handle extreme vacuum of under 50mTorr. This jar was placed in a -80C° freezer for 24 hours to allow a deep freeze to occur. The jar is then taken and attached to the manifold of the lyophilizer via a specialize top for the jars. This process is shown in Figure 2.5. A ball valve on the manifold is opened and the jar is placed under vacuum,

allowing the water to sublimate off the CNF sampled and collected into the condenser of the lyophilizer. The samples were freeze dried for 72 hours to insure complete dehydration. When drying completed the ball valve was closed and the jar taken off the manifold. The CNF solids were then collected from the jar and used for further testing and characterization.

2.3. Results

2.3.1. Bulk Water Content as a Function of Time

With the lyophilization process further understood, it is confirmed it will be an integral part in the process of create porous CNF solid forms. The water content of the CNF is monitored

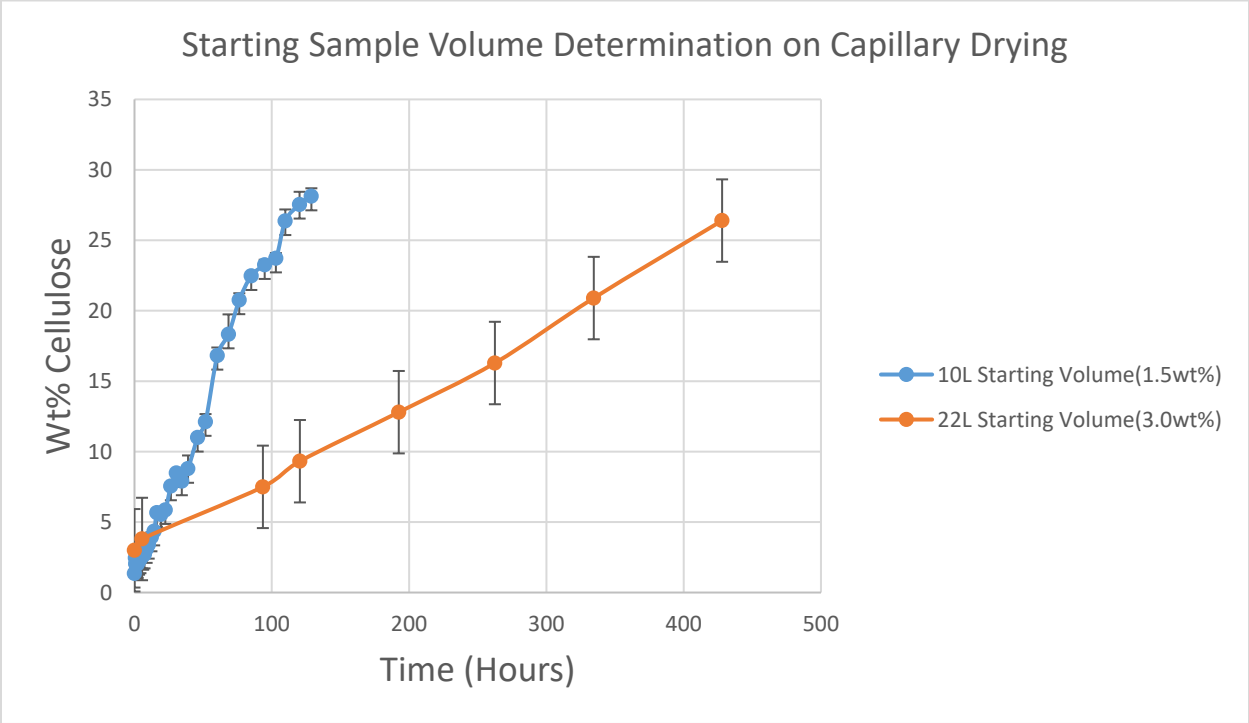

Figure 2.5 Comparing drying rates of separate CNF samples of different starting volume and wt.% fiber. As expected, samples with less initial water volume dehydrated at a higher rate. Further experimentation would be needed to identify the full effect of the two independent variables, starting volume and starting wt.%, on drying rate.

throughout the drying process via a moisture content balance. Small samples of the nanocellulose fiber were collected from the drying mold at uniform time intervals and placed into the specialized balance for a moisture measurement. Some trial result can be examined in Figure 2.5.

Both trials were run under ambient conditions, 25 degrees Celsius and atmospheric pressure. Comparing these two trials shows the rate of drying was much greater in the sample with a smaller initial volume and initial fiber percentage. More trials are needed to identify the contribution of the two independent variables to the dependent variable of drying rate. It can be observed the Y-axis only expands to 30 wt.% Cellulose fibers. This is a limiting factor in experimental data collection. When the Nanocellulose Matrix approaches a fiber percentage of 30; it becomes too difficult to manually remove fiber from the bulk matrix. At this point, moisture content balance is no longer a viable option to measure the water within the CNF matrix. From this point forward in experimentation, the volume of the sample was used to estimate water content of the matrix

Additionally, it is noted under ambient conditions drying times are too long for practical production of medical material in an industrial setting. To confirm the drying time will decrease in a heated environment, drying trials were run in a walk-in convection oven at 100 degrees Celsius on a 10L volume of CNF slurry. This was compared to drying times of 10L of CNF under ambient conditions. As expected, CNF drying times were greatly decreased when thermal energy is added to the system. These trial comparisons can be seen in Figure 2.6. The CNF sample that was heated dewatered at a maximum rate of 3.125 wt.%-water/hr. This is an increase over the 0.909 wt.%-Water/Hr. under ambient conditions. This caused the heated sample to contain less than 10% water within 30 hours of drying. This time scale is more reasonable for production of a material with medical applications.

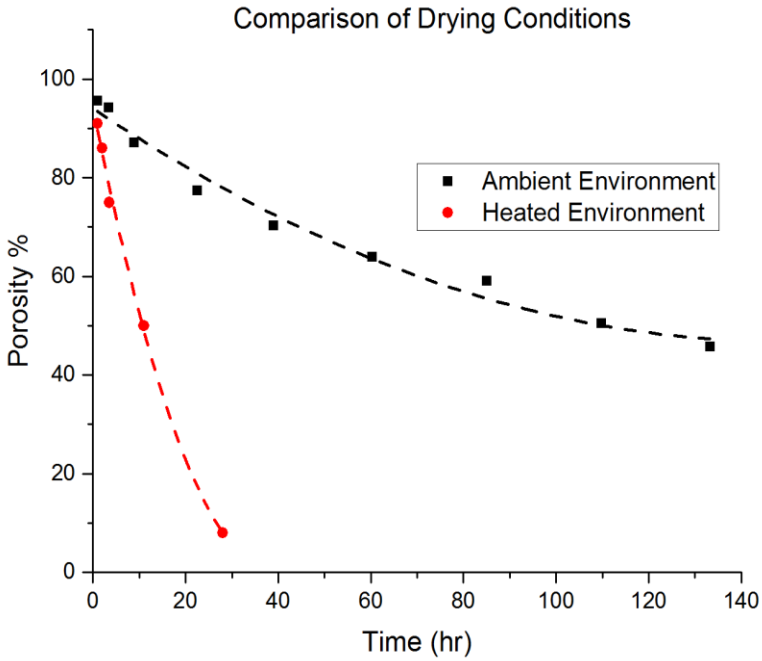

Figure 2.6 Comparing drying rates of 10L CNF samples when under ambient and heated conditions (100˚C). As predicted when designing experimentation, the heated sample dried significantly fast than the ambient sample.

Further drying trials were run to examine the drying properties of the brick mold. A trial was executed to experiment with the idea of a two phase drying process. First under ambient conditions and then a later transfer to a heated environment. The two phase drying would allow electricity to be saved during the production process if an industrial scale were to be reached. A 22L CNF sample was left to dewater at ambient conditions for 334 hours. Enough time for dewatering via capillary action to decrease to a low rate. Failing to significantly overcome the energy barriers within the system. The main barrier being the increased hydrogen bond hydrogen bond availability between water and cellulose fibers.

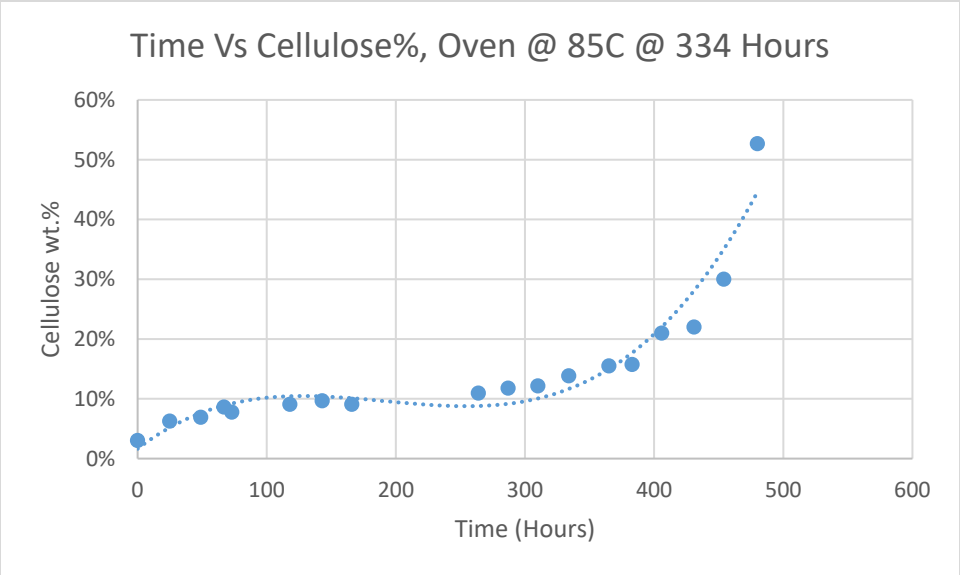

Figure 2.7 Two phase CNF drying experiment to determine drying rate dynamics and feasibility ambient-heat 2 step drying

It can be observed in Figure 2.7 that this energy barrier occurs at 10% wt. CNF. Something that failed to occur in the data of Figure 2.5. This can be explained by the relative humidity in the air. This experiment took place within the Technical Resource Center at the University of Maine during the summer months. Not only is the TRC not properly climate controlled or insulated, but Maine's summers are extremely humid. According to NOAA(National Center for Environmental information), the average relative humidity for the month of July in the Bangor area is 81% The data in Figure 2.5 was gathered within a laboratory that most likely contained a low relative humidity. Once the wt.% was determined steady, the mold was moved to a walk in oven with a temperature of 85˚C. It can be noted on Figure 2.7 that the de-watering rate increased under the increased thermal conditions beginning at 334 hours. Overall this experiment shows a two-step drying process is feasible.

2.3.2. Visual Inspection

Shortly after the slurry was added to the mold, multiple physical observations could be made. Within 30 seconds, water could be observed reaching the brick-air interface on the outside of the mold. Within the first 5 minutes, the level of the CNF slurry can be observed decreasing in level. Suggesting a significant quantity of water is being withdrawn from the system via the

B) A)

Figure 2.8 A) CNF adhering to the inside walls of the brick molding. The majority of the bulk material can be seen centralized at the mold's bottom. B) The capturing pan outside the mold, containing an inch of water. The pan requires periodic draining.

capillary. Over the course of multiple days more physical observations are made during the drying process. As the water content of the bulk CNF decreases, the volume within the mold decreases as well. Decreasing volume of the bulk material causes stray CNF to adhere to the porous surface

of the brick. This phenomena is cause by negative pressure created by capillary air-water interface within the brick represented in Equation 2.2. The capture tray underneath the mold filling with water can also be observed. The capture tray is used as a temporary method to quantitatively track dewatering of the CNF bulk material. These physical occurrences can be seen in Figure 2.8.

A significant color difference was noted between dry CNF of the porous variety and CNF of a higher density. Porous CNF is stark white in color, whereas dense CNF is tan. This contrast can be explained optically as cellulose is a very efficient at scattering light. However, light scattering is very concentration dependent. The more porous the cellulose matrix, the less concentrated cellulose is as a bulk material; there for creating a change in optical scattering. There are experimental advantages to this color change. The contrast in color allows for differences in the porosity of a sample to be observed qualitatively after the freeze drying process.

Figure 2.9 Surface binding phenomena represented in a freeze dried CNF sample. The density profile of CNF dried in this manner is similar to the profile of human bone; a dense outside layer with a porous center.

Pore size distribution with select CNF solids can be identified before qualitative examination is performed. As a result of this method, it was further observed the tan, dense CNF initially forms at the CNF-air interface exclusively. This can be explained by the characteristics of interfacial energy. Molecules on the surface of a material inherently have greater energy than molecules within the bulk. Because the CNF-air contains greater energy it is expected that that pores will collapse and greater hydrogen bonds will from in this regime. The collapse of pores and increased hydrogen bonding at the interface can be observed in Figure 2.9. The current profile created from drying may prove to be advantageous as the pore profile mimics the porous profile of human bone; with a dense outer layer and a more porous center. Harnessing this physically phenomena could prove important for future research.

The pores formed within nanocellulose fiber solid forms are not exclusively on the micro and sub-micron scale. Larger pores are capable of formation because of cavitations created when adding energy to the system. These large cavitations are created by spontaneous vaporization of water within the fibrous matrix as the matrix is being dewatered to a solid state. This energy can be created via a change of temperature or pressure. These cavitations significantly decrease the density of the CNF solid; creating a porosity of 20% on average. Despite the decreased density, material strength is not negatively affected in a noticeable, qualitative way. Examples of this cavity affect can be seen in Figure 2.10. It is important to note the visual similarities between cavitated CNF and cancellous (spongey) bone. It is reiterated that the ideal bone analogue would have density control as the body has over human bone. Mimicking the cavities and large pores of human bone could be an efficient approach to solving this medical problem. Cavitation production was successful in both bare CNF and CNF doped with Iron oxide nanoparticles. Qualitatively it

A)

B)

Figure 2.10 A) Cavities within a tab of CNF doped with Iron Oxide Nanoparticles. B) Cavities within an ingot of bare CNF.

is observed iron oxide nano particles increase the cavity effect within CNF. Further trials must be run to confirm causation between the two variables.

2.3.3. Pore Size Distribution in Relation to CNF Porosity

For any biomaterial with biological application, pore size and structure are of paramount information when attempting to characterize and model a material system. Research shows epithelial cells have the ability to permeate pores as small as 2 microns in diameter. Thus giving a lower limit goal of pore size for an ideal biomaterial system requiring normal cell ingrowth. Because of the large size of osteocytes, a bone analogue material for ingrowth requires pores larger than 2 microns. On average, osteocytes have a width of 15 microns and a depth of 7 microns.[28] According to studies, a bone analogue capable of allowing bone cell ingrowth and replication

would require pores the size of 600 microns for adhesion and ingrowth. With this in mind, the current goal for CNF are 300 micron pores. This is chosen as a conservative goal that can be

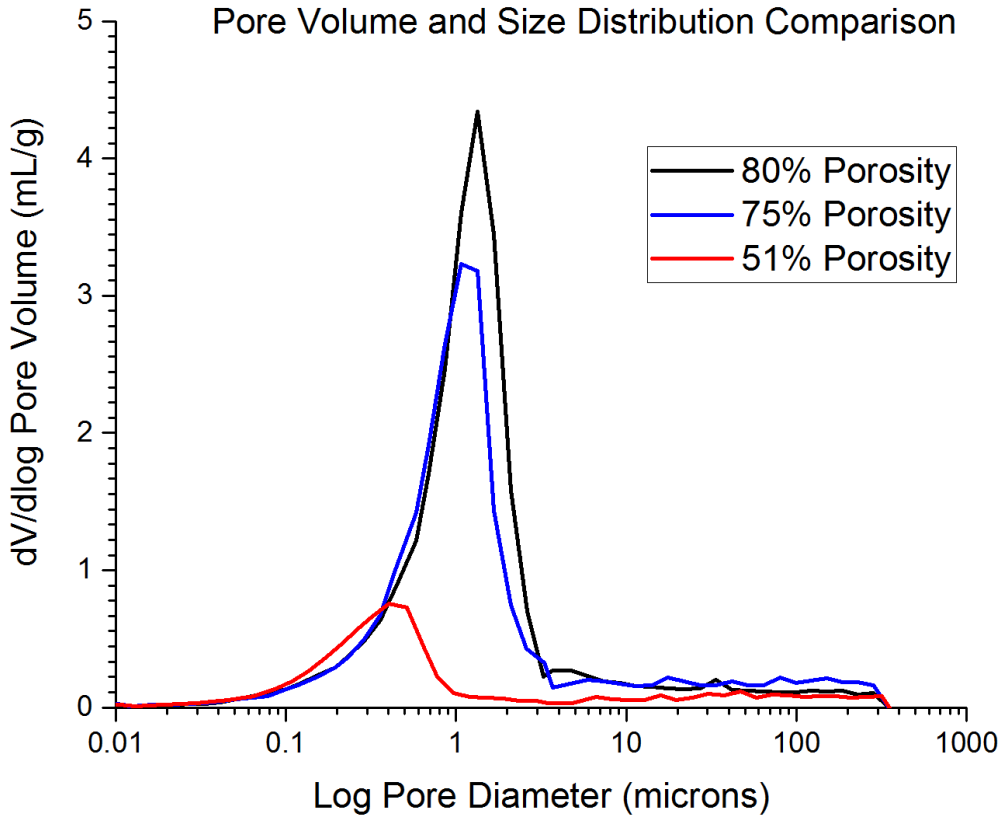

Figure 2.11 The pore size distribution of CNF at different overall porosities. Results suggest pore size decreases as porosity decreases. This suggestion is physically logical as water removal allows fibers to become closer together, decreasing pore size.

improved upon. Larger pores are paramount because of necessary mass transport of nutrients to the inside portions of the material matrix.

The pore size distribution of the CNF produced required examination because of the aforementioned engineering constraints. To accomplish this, a Mercury Porosimeter was used on small CNF samples of varying porosity. A mercury porosimeter pressurizes a chamber full of the

desired sample and mercury. It then measures the rate of mercury displacement into the pores as the pressure of the chamber is increased. The porosimeter uses these displacement rates to calculate the pore distribution within a sample. The smaller the pores, the more pressure is needed to displace the mercury. This measurement was only performed on four samples because of instrument difficulty. The 7% porosity sample was removed from Figure 2.11 as the minimal pore volume of the sample created significant uncertainty with the measurement. The overall volume was several orders of magnitude lower than the remainder of the samples tested.

When observing figure 2.11 there are three important factors to note. Firstly it is observed that using the current freeze drying technique, the pore sizes that result are significantly mono disperse. This control of a narrow size distribution is important for engineering biomaterials following specific design constraints, a proper bone analog is one example of this. These data suggest observed monodispersity remains intact as porosity decreases. This trend is probable as more organized, free energy hydrogen bonding is occurring between the fibers as the matrix dehydrates and collapses; causing similar variance of pore sizes as observed in the 51% porosity sample. Secondly, it suggests observed average pore size decreases as porosity decreases. This trend is probable because as previously stated, decreasing porosity means pores within the matrix are collapsing. With collapsing pore, it is understood that the average pore volume will decrease with certainty. Lastly and paramount to the experiment, Figure 2.11 suggests current production methods of CNF create a pore structure that is too small for ingrowth or adhesion of osteocytes. CNF at 80-75% porosity are centralized around 1 micron pore distribution. This is significantly smaller than the initial goal of 300 micron. This result suggests changes to the current production process are mandatory if osteocyte ingrowth is to be an achievable goal.

2.4. Discussion

Overall, the drying of the cellulose nanofibers was an extreme success. Drying of the CNF in a controlled, tunable manor was achieved. The process was controlled enough that hydrogen bonding of the cellulose fibers, which yield strength, were not compromised. However, the process is still viable for industrial throughput of a biomedical material; which can be as low as 1000 screws a month. The controlled drying rate enabled a selective measure of creating CNF solids of a selected porosity. As discussed previously, material porosity control is an important factor for developing a successful bone analog. Human bone consistently differs in both density and porosity depending on the necessary application and where in the body it is located. It is suggested because flexural modulus of bone changes with density and porosity, that CNF will have similar structural relationship. Material strength testing will be performed to confirm if CNF flexural modulus and strength can be controlled as a result of porosity control.

CHAPTER 3

CNF MECHANICAL STRENGTH & CHARACTERISTICS

3.1. Introduction

As suggested previously, significant masses of CNF fibers may be dewatered efficiently as the porosity is controlled via tunable methods. Porosity control represents the adjustable density desired for any bone analog replacement. The second characteristic desired is Young's Modulus which is fully compatible with human bone. The evidence is required to suggest CNF will not induce an environment of stress shielding. Inherently, Young's Modulus of the new CNF solids must be characterized. To achieve a measurement of Young's Modulus a three point bend test must be performed. For the application of CNF, Young's Modulus must be measured as a factor of porosity. A large range of porosities is to be examined and characterized. In addition to the elastic modulus; the hardness of the material requires characterizing. A material used in the biomechanical application must withstand repeated sheer stresses over long periods of time *in vivo*. Mohs hardness of CNF solids will be identified via a Mohs scale of hardness kit. This method will allow the hardness of CNF to be compared with numerous biomaterials currently in use.

3.2. Methods

3.2.1. Mohs Scale of Hardness

The Mohs Scale of Hardness is typically an important test performed on minerals to test relative hardness and identify the tested material. The test compares the examined material to 10 known reference materials. Scratch tools made of these reference materials are the most common way to interpret Mohs Hardness. Figure 3.1 shows a typical Mohs Hardness kit with the aforementioned scratch tools.

Figure 3.1 Mohs Scale of Hardness kit with included scratch tools. The size of the number labeled indicates hardness. Tool #2 is a polymer whereas tool #9 is a dense metal alloy.

The procedure is qualitative and concise. Using the scratch tool on a level testing surface, strokes back and forth are made using firm pressure. When observing the results the following factors are considered:

1. If specimen A can scratch specimen B, then specimen A is harder than specimen B.
2. If specimen A does not scratch specimen B, specimen B is harder than specimen A.
3. If both specimens are of the equal hardness they will be inefficient at scratching one another; any visible markings must be able to be rubbed away to confirm identical hardness.
4. If specimen A is scratched by specimen B but cannot be scratched by specimen C, then the hardness of A is between B and C.

An example of factor 1 is represented in Figure 3.1; where material #3 (copper) has visibly scratched and displaced material on a smooth CNF surface. 11 tabs were tested in total, all ranging from 3-80% porosity.

Figure 3.2 #3 Copper scratch tool creating observable markings on the smooth 6% porosity CNF surface; indicating CNF is lower than 3 on the Mohs Hardness Scale.

3.2.2. INSTRON 3-Point Bend Flexural Test

The three point bending flexural Test is the most common test in the industry to determine materials: elastic modulus (Young's Modulus), flexural stress, flexural strain, and flexural stress-strain response. From this, it is determined the Three Point Bend Test is the optimal method of acquiring the Young's Modulus of the CNF solids. An INSTRON 5500R was the instrument used

to perform the tests. The instrument setup is shown in figure 4.3. The procedure requires the tested material be formed into tabs with at least a 1:16 thickness to length ratio. The required tabs are machined using a mill and drop saw from dewatered CNF ingots.

Figure 3.3 INSTRON 5500R load frame with an INSTRON 4202 base.

Three-point bend tests on INSTRON instruments fail to give measurements of elastic moduli. In contrast, the INSTRON Bluehill® software calculates the flexural modulus of elasticity from the stress-strain curve. The Flexural Modulus equation is represented by Equation 1.

$$E_f = \frac{L^3 m}{4bd^3}$$

Equation 1. Flexural modulus of elasticity

L= Support span (mm)

b= Width of test beam

m= Slope of the initial load deflection curve

d= Depth or thickness of the deflected tab or beam

The 1:16 d to L ratio of the tab is paramount in the experimental procedure. If Equation 1 is observed it is noted that E_f goes to infinity is Length increases and depth decreases. A small depth and large length ensures E_f is the largest term in the function for Young's Modulus. 11 tabs were tested in total, all ranging from 3-80% porosity.

3.3. Results

High porosity CNF failed to indicate significant toughness during Mohs hardness testing. The polymer scratch tool, Material #2, successfully created visible displacements in the material of 70-80% porosity. This creates an observation of factor #1, that the polymer is harder than the porous CNF. This suggests high porosity CNF has a Mohs hardness of less than 2. From these observations, we interpret high porosity CNF is a 1.5 on the Mohs scale of Hardness. Material #2 failed to mark the dense, low porosity CNF; leading to the observation of factor #4. Material #3 successfully displaced and marked the high-density CNF; this can again be seen in Figure 4.2. This leads to the observation of factor #1. Using these observations we interpret CNF with

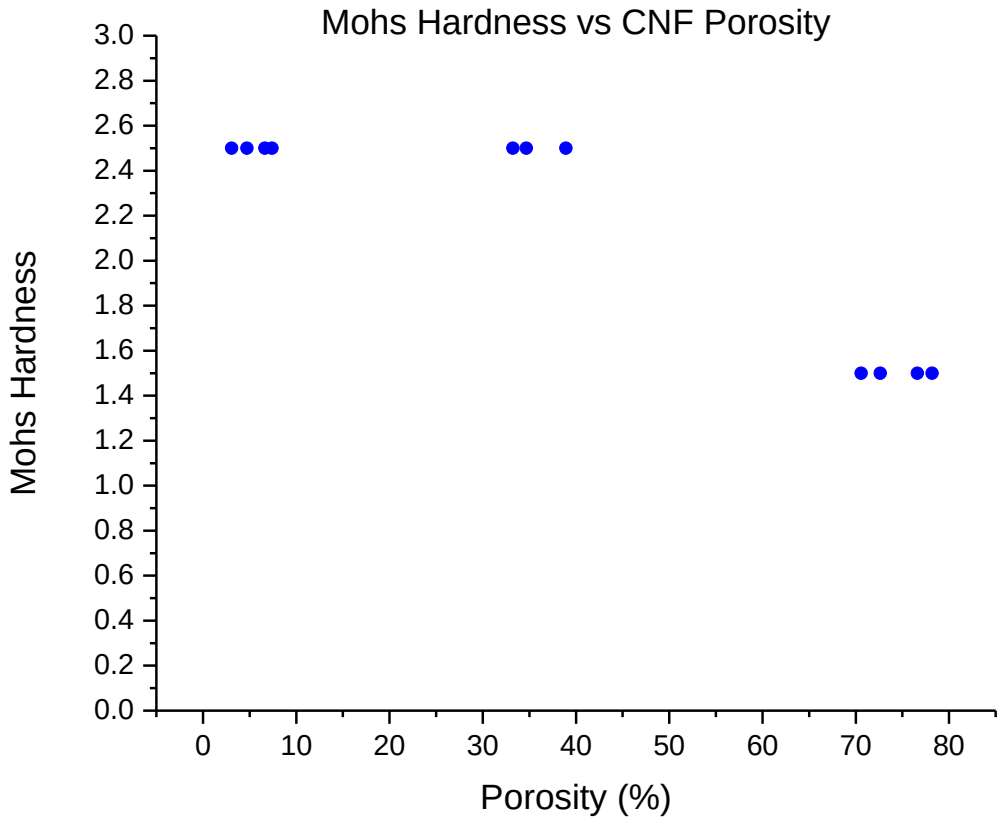

Figure 3.4 Mohs hardness of CNF in relationship to porosity. The qualitative flaws of Mohs hardness can be observed as well as the simple trend: As porosity increases, hardness decreases.

porosities of 40-3% are a 2.5 on the Mohs scale of hardness. The suggested porosity-hardness relationship is represented in Figure 4.4. As with the Mohs hardness testing, results of the three-point bend test suggest a similar strength-porosity trend. The flexural modulus of 11 samples of varying porosities (5-78%) suggests a linear relationship of flexural modulus vs porosity. However, a function of a different variety cannot be ruled out. These data are represented in Figure 3.5. The Flexural Modulus of the material ranged from 177.36MPa to 6323.74MPa.

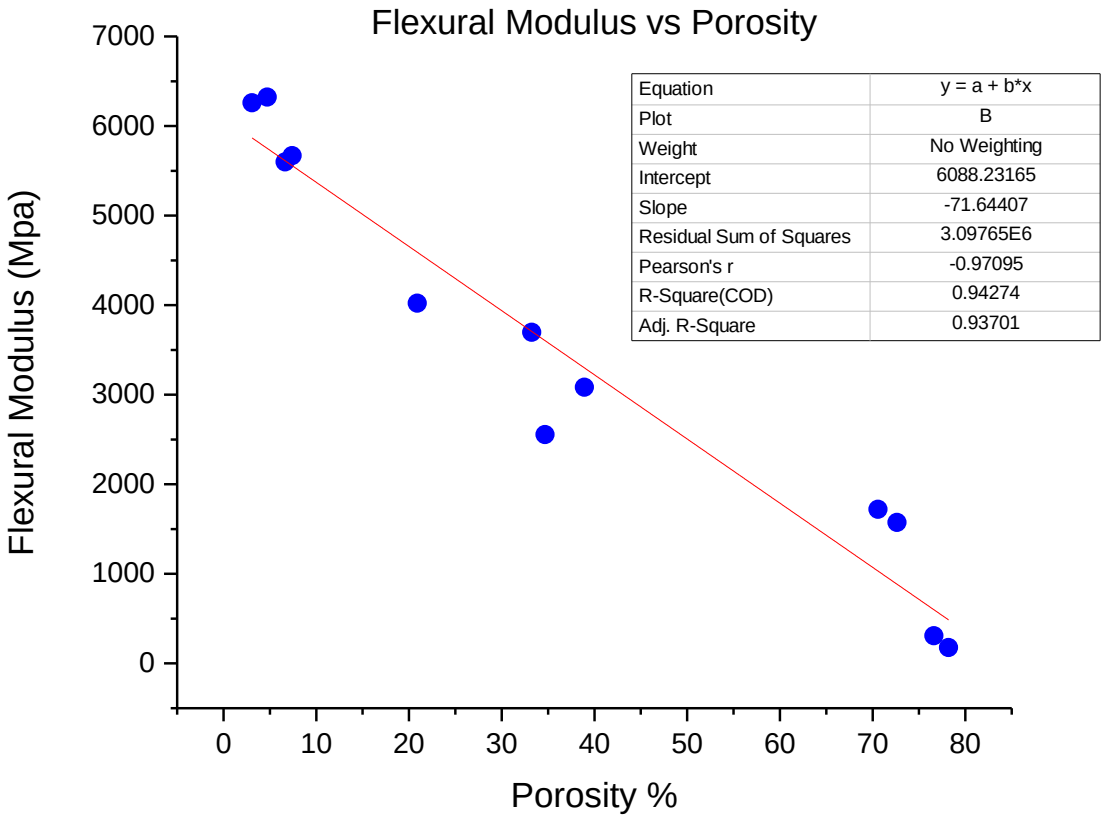

Figure 3.5 Three-point bend tests indicate a clear relationship between Flexural modulus and porosity. The relationship suggests linearity with an R-Square value of 0.94. However, another fit may be optimal with more sample data.

Qualitative observations of the bend tests indicated tabs of greater porosities have greater flexibility before failure. The ability of the material to deform is inherently represented by the Flexural modulus. Low flexural modulus indicates bending under lower stresses. As expected, all high porosity CNF had lower Flexural modulus and higher observed flexibility during testing. Low porosity CNF possesses a higher flexural modulus and lower observed flexibility during testing.

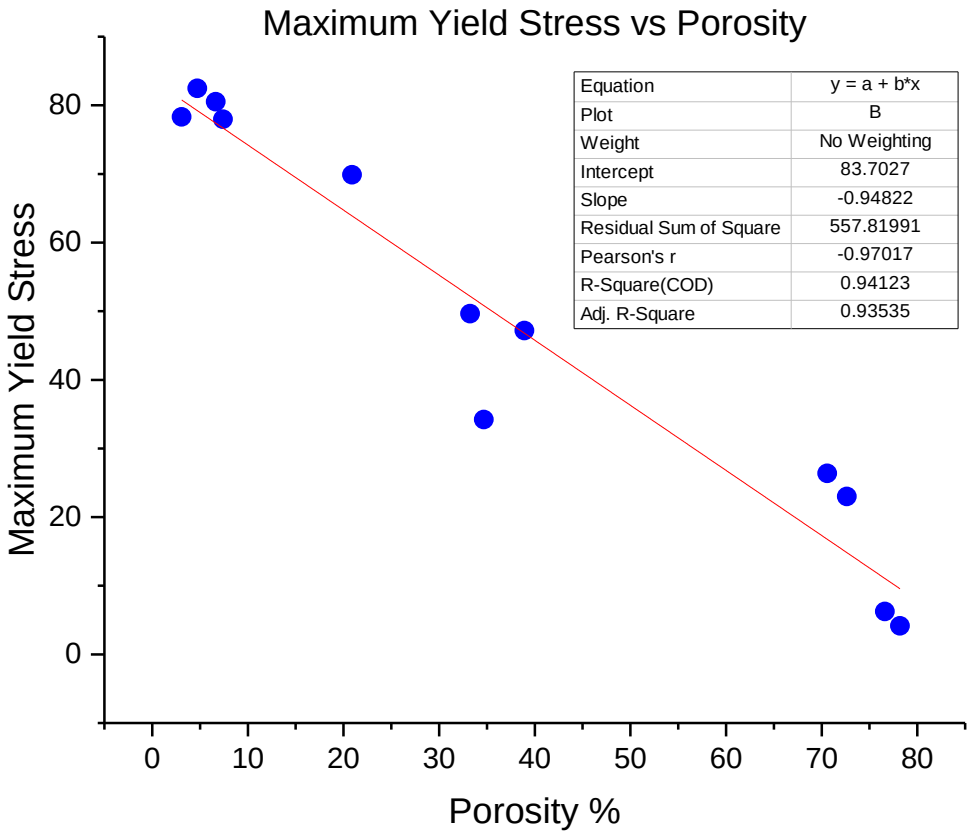

Figure 3.6 The graphical relationship of CNF porosity and maximum yield stress before failure. The data suggest a linear trend similar to the Flexural Modulus-porosity relationship. Further testing is needed to confirm this fit.

Additionally, three-point bend tests measure maximum load and maximum yield stress of each sample. Maximum yield stress is the amount of stress a material can undergo before deforming plastically. In the majority of cases, this indicates a mechanical failure. The tests on the same 11 samples suggest a similar, linear relationship between porosity and yield stress. Once again, a greater sample population is needed to confirm the relationship.

3.4. Discussion

Pure CNF has shown great potential as a biomaterial. However further testing has identified drawbacks and flaws within its characteristics. Mohs scale of hardness testing identifies the hardness of low porosity CNF as similar to an engineered dense polymer. Test results are reflective of reality, as low porosity CNF is a tightly packed polymer structure. Dense polymers are typically not ideal for long term use within a moving joint. UHMWPE (Ultra-high-molecular-weight-polyethylene) and PTFE are exceptions due to a small coefficient of friction. Although not quantified, it is acknowledged CNF in a biological environment will not have a coefficient of friction on the level of PTFE and UHMWPE. Rehydration and swelling of the cellulose matrix are currently a critical issue in this regard. Swelling of the CNF causes weakening of the hydrogen bond along with increased surface roughness.

Three-point bend testing strongly suggests Young's modulus tunability of pure CNF solids. Porosity control of the polymer matrix allows a wide range of material strength and properties to be achieved. In figure 4.7 the density and Young's modulus of the CNF samples is compared to known materials that comprise human bone. The data suggests pure CNF can achieve the density and Young's Modulus of collagen and cancellous bone when porosity is varied. This is an important and advantageous characteristic as the cancellous bone has a large range of densities via varying porosity. This creates difficulties in making a successful cancellous bone analog. The tunability of CNF porosity creates an ideal analog for this system. Represented again in Figure 4.6; the physical relationship of CNF density and Young's modulus follows a similar mathematical curve as cancellous bone density vs Young's modulus.

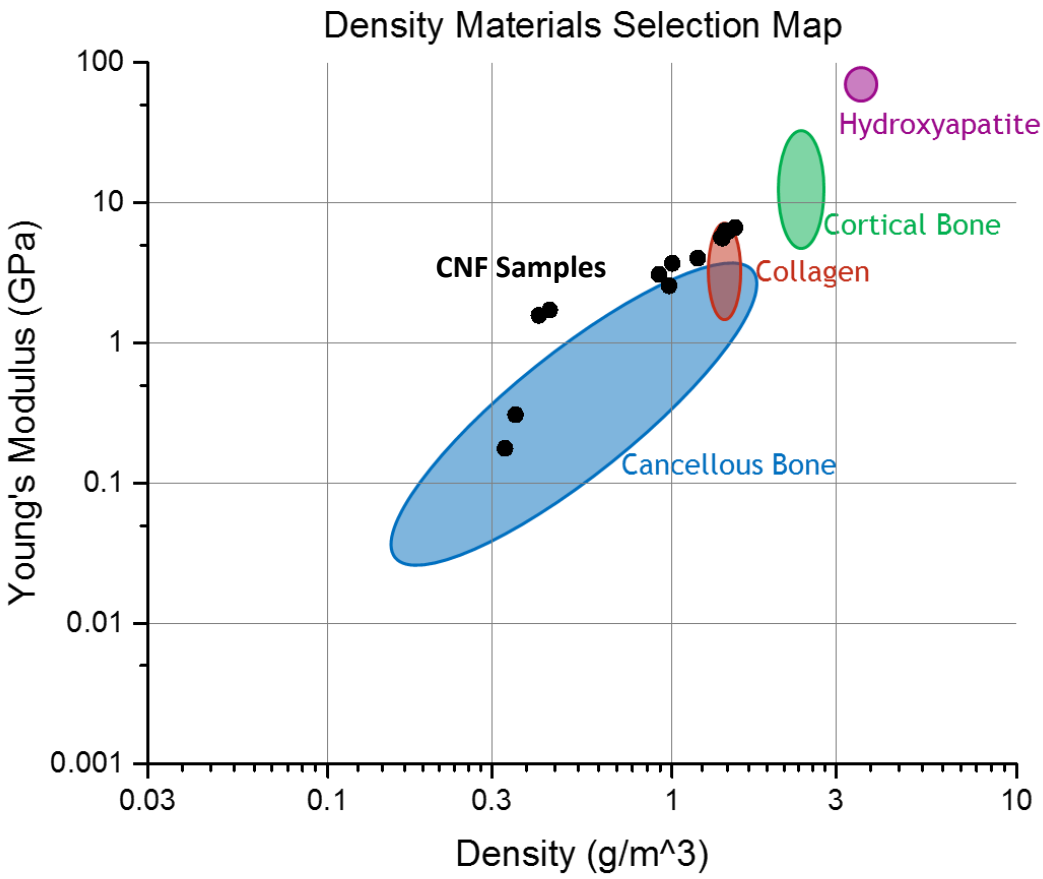

Figure 3.7 Young's modulus vs bone material density. Results of the mechanical testing compared with known values of bone components. Pure CNF reaches identical mechanical values of both Collagen and bone at various porosities.

The dense CNF forms mimic collagen protein density and Young's Modulus with great accuracy. Along with similar mechanical characteristics, collagen and CNF have similar physical characteristics and nanostructure. Although collagen is a protein matrix rather than a polymer matrix; both are collections of fibers with diameters of less than 200nm. These physical similarities can be observed when SEM images are compared. The immediate similarities between CNF and collagen are once again advantageous for the application of cellulose nanofibers. Collagen is the most abundant protein in mammals and makes up 25-35% of mammalian protein content. Collagen makes up approximately 20% of bone mass, lowers bone Young's modulus;

inherently providing the flexible properties of mammalian bone. Additionally, collagen makes up the majority of cartilage and connective tissue such as tendons and ligaments. The human body organizes collagen matrices differently according to different mechanical applications. These applications include rigidity (bone-protein matrix), elasticity (cartilage), and flexibility (Tendons). Low porosity CNF shows characteristics of elasticity and rigidity. Further testing is needed to explore CNF-cartilage analog possibilities.

It is suggested slow formed high density CNF represents the strongest material pure CNF can produce when dehydrated. Theoretically, the most hydrogen bonding has occurred in this state; inherently producing maximum mechanical strength. The pure CNF samples failed to reach Young's modulus of dense cortical bone and hydroxyapatite. This data suggests pure CNF is not an optimal bone analog for high density and force loaded bone. Hydroxyapatite, the mineral component of mammalian bone, provides strength and creates the brittle properties bone possess. As a polymer matrix CNF inherently lacks the physical and mechanical characteristics of hydroxyapatite. Hydroxyapatite lacks the elasticity and flexibility of CNF and collagen. Mammalian bone is a composite material because it requires strength and elasticity that no sole material can provide. Although testing suggests CNF can replace the fibrous matrix component of the composite that makes up bone; the data suggests it will not possess all the mechanical characteristics required for a full bone analogue.

Although CNF does not show overwhelming promise as a standalone structural bone analog, it shows great potential as part of a bone composite. A cancellous bone analog additionally shows promise. Further mechanical testing is needed to determine new CNF applications and for full characterization of both dense CNF and CNF of varying porosities. Further research should be examined with CNF-hydroxyapatite interactions and possible composite materials. It has been

shown that hydroxyapatite crystals can be grown on electro spun, phosphorylated CNF in simulated biological fluid.[21] However, the CNF samples tested were significantly small volumes and mass amounts. Mechanical testing of these samples would be impossible on an INSTRON device. It is of high interest that this chemistry is tested with the large volume CNF forms that are produced by the University of Maine. With large volume CNF forms, a similar experiment should be completed to determine possible mechanical changes and application of the new material. A CNF-Hydroxyapatite, or tri-calcium phosphate bone analog in large volumes would be an exciting, novel material. Additionally, it is recommended that CNF-osteoblast studies be further investigated.

CHAPTER 4

MACHINING CHARACTERISTICS FOR ORTHOPEDIC APPLICATION

4.1. Introduction

Because small scale production of CNF solid forms have been accomplished and deemed viable for Biomedical and orthopedic applications, machinability of the material must be examined. Many polymer material platforms used for orthopedic applications are processed to usable solid forms via sintering or injection molding. Because CNF as a polymer is not capable of injection molding and unable to be sintered in wet slurry form; alternative measures are required for this platform. Currently, the most viable method is to dry the CNF slurry to dense plastic and machine this plastic into the desired shape and form. This process is subtractive manufacturing. Machining via automated units is as reproducible and consistent as the alternative molding processes. CNC machines use 3D CAD files designed by the inventor using computer software. The 3D CAD file is uploaded into the CNC device and using multiple milling bits the material is cut and machined into the desired shape from the CAD file. For this method to function, the mechanical properties of CNF must withstand the sheer stresses and strains created by the mill bits while machining. The mechanical properties of CNF will also dictate the resolution capabilities of the machining process i.e. Thinner threads require more stiff and resilient material than thicker threading. Inherently, the milling and CNC capabilities of CNF need further study. This will be done using two different methods. Firstly, a quantitative measurements of compressive strength and tensile strength must be done. Secondly, a qualitative experiment will be perform; milling and lathing the material using these instruments by hand and observing these results.

4.2. Methods

4.2.1. Quantitative Compressive and Tensile Strength Testing

Figure 4.1 A typical INSTRON setup for testing the tensile strength of a material. The CNF was machined to tabs for more efficient and consistent testing. (Image curtesy of University of Maine Mechanical Engineering)

When qualitatively examining a materials machining capabilities, the tensile and compressive strength of the material must be investigated. Not only will this information be important for this application, but additionally supplement previous mechanical testing done for Young's Modulus. To measure tensile strength, an INSTRON 4202 was set up with two vertical tension clamps. CNF within these tension clamps can be viewed in Figure 4.1. CNF was machined to tabular form. The dimensions of these three tabs were approximately 94mm in length, 20mm in

width, and 6.5mm in thickness. Sandpaper was placed between the CNF tab and the clamp surface to insure a no-slip condition during experimentation. When using the INSRON software the Fiberglass Reinforced Plastics (FRP) test program was selected. This is thought to best represent CNF as the two materials have similar Young's Moduli. The experiment was performed until the material failed and completely broke apart.

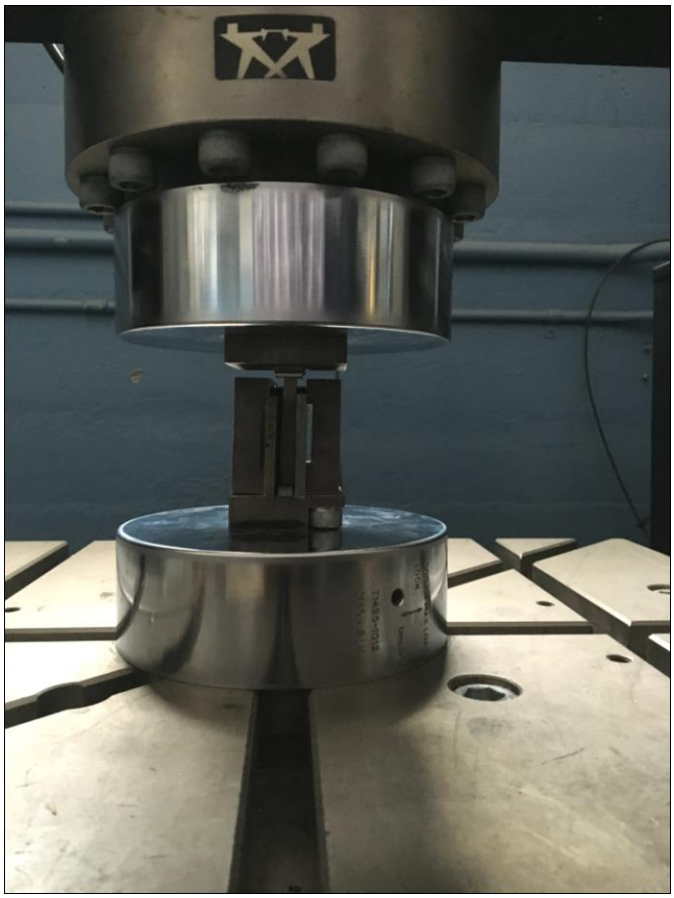

Figure 4.2 Compressive testing setup on the 4485 INSTRON device.

CNF compressive testing was performed on a separate 4485 INSTRON device. For compressive testing, a CNF tab of a difference length was needed. Three new tabs were fabricated with the following dimensions: 45mm length, 25mm width, and a 6.5mm thickness. These tabs can be observed in the compressive clamp within Figure 4.2. Once again it was assumed CNF response similar in a mechanical fashion to FRP when selecting a program type within the software. The trials were run until the operator noted that there is a spike in strain, indicating compressive failure of the material.

4.2.2 Qualitative Machining of Material

The initial machining of CNF will be done by tools controlled by human hand. This will provide operator feedback and additional anecdotal evidence to the machinability of the material. The machinist will create at least one screw and one threaded pin out of CNF. More thread types will be attempted if time is available. The initial fixation screw will have a 1/4 inch OD and ¼-20 thread size and count. This is considered a general thread type for machining, containing shallow threads for easier lathing. If initial machining is successful, a 3D CAD design will be constructed using SOLIDWORKS software for CNC device implementation. The CNC process will be carried out by the Advanced Manufacturing Center on The University of Maine campus. This initial design

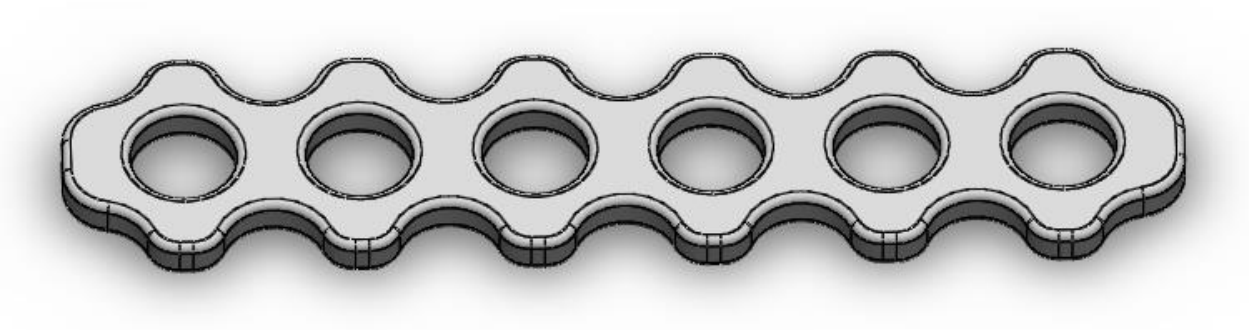

Figure 4.3 3D CAD of design #1 for a CNF bone fixation plate 80mm in length, 17mm wide, and 2mm thick. The screw holes are ¼ inch. This simple, straight design will be ideal for preliminary CNC testing.

will be a simple bone plate of significant thickness (2.3mm vs the standard 1mm). CNC machines excel in more flat, two dimensional designs. For this reason, a bone plate shape is preferred over a screw or pin when considering the practice of CNC fabrication.

If preliminary machining proves successful with personal and CNC machining, then a second phase of machining will be implemented. This phase will consist of orthopedic devices that are more difficult to machine because of lower dimensional tolerances. These smaller dimensions will cause less stress absorbing material to be available, increasing the chances of material failure under machine stress. The machinist will mill and lathe a threaded orthopedic pin and a smaller, tapered, interference screw; typically used for ACL reconstructive surgeries. Two further CAD designs will additionally be created on SOLIDWORKS for CNC manufacturing. The first design will mimic the plate in Figure 4.3, however, will be 1mm in thickness. This 1mm thickness is of paramount importance as this mimics titanium bone plate dimensions currently used in the medical field. The second CAD design is a more complex bone plate and can be observed in Figure 4.4 and Figure 4.5 It will contain a three dimensional, 45 degree contour for smaller bones such at the metacarpals of the hands or metatarsals of the feet. Holes for fixation screws will also be offset for better distribution of force.

Figure 4.4 3D CAD design #2, a more complex and irregular design for a bone fixation plate. The wings add additional length and width over design 1. The screw holes are ¼ inch. This design will further test the CNC capabilities of CNF with less thickness and a 45 degree contour.

Figure 4.5 View of the 45 degree contour designated to the wing of design #2. This angle helps contour around the bone being fixed in place. The elastic properties of CNF will help handle the three points of stress from the wing screws.

4.3. Results

4.3.1. Quantitative Compressive and Tensile Strength Testing

Compressive and tensile stress testing yielded significant results concerning material characterization. Resulting data from compressive stress-strain testing can be observed within Figure 4.6. The results suggested nanocellulose fiber has a yield compressive stress, also known as compressive strength, of 25-30 MPa, approximately 4000psi. High density polyethylene (HDPE), an extremely mechinable polymer, has a compressive strength of 20 MPa. Therefore qualitatively suggesting the machinability of CNF should be comparable or better to HDPE in terms of compression.

An initial characteristic to observe in Figure 4.6 is the viscoelastic property of CNF. Because bone is a composite material made up of brittle hydroxyapatite and elastic collagen, it is inherently viscoelastic and contains both physical properties.

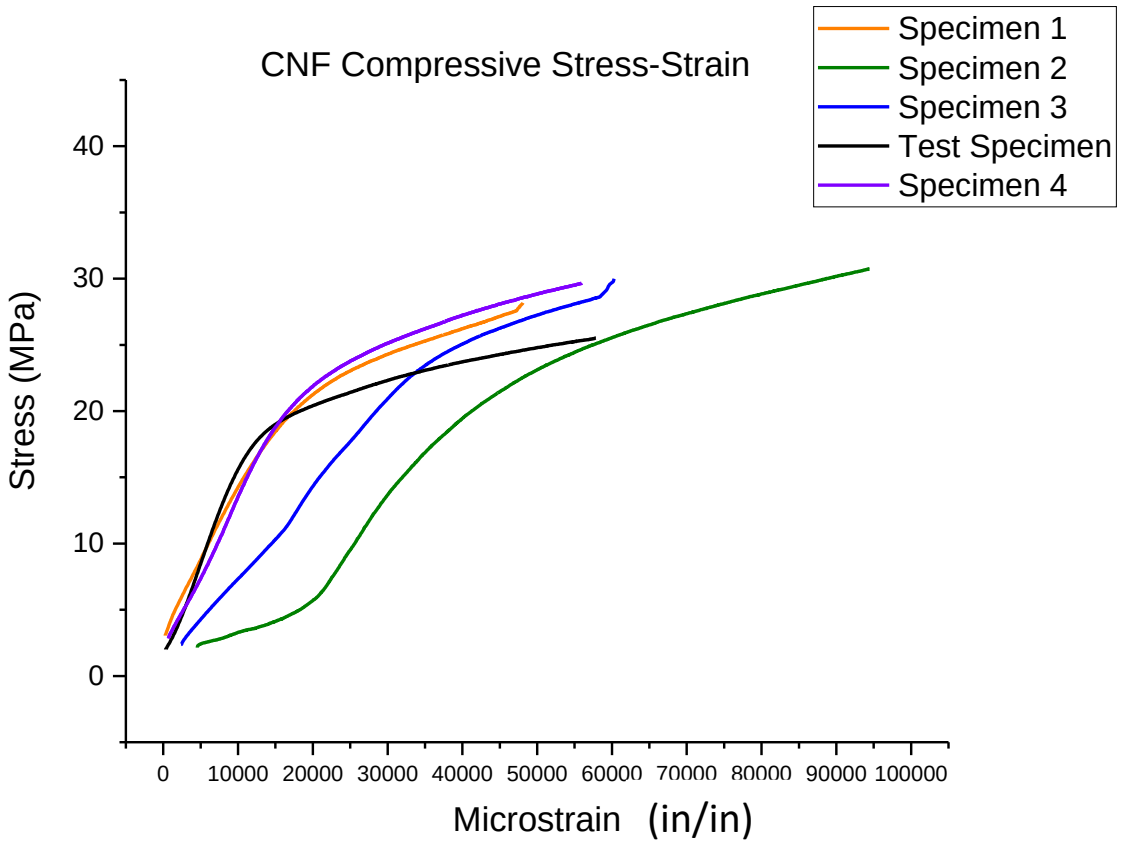

Figure 4.6 Compressive stress-strain curves for five samples of CNF tabs. Each tab had a 45mm length, 25mm width, and a 6.5mm thickness. The results suggest CNF has a higher compressive strength than HDPE.

Tensile stress-strain data collected from the three CNF tabs can be viewed in Figure 4.7. Results of testing were equally as impressive as those for compressive stress; suggesting high density CNF has a tensile strength of 25 MPa. This further suggests CNF has a tensile strength comparable to HDPE, a gold standard for mechinable polymers. CNF possessed both tensile and compressive strengths that suggests it is well capable of being machined as a standard polymer.

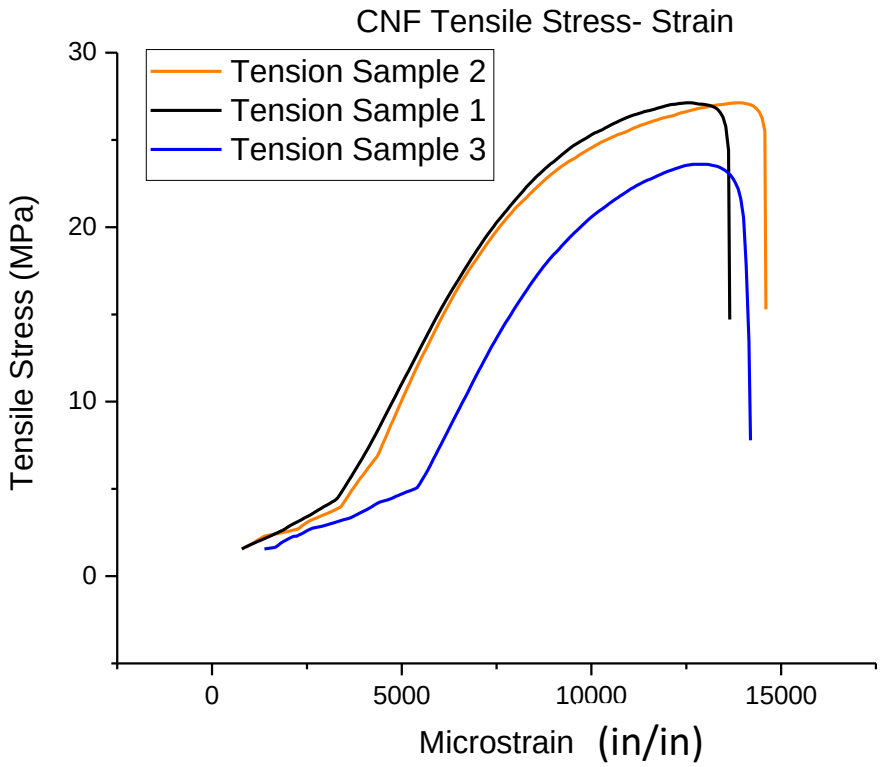

Figure 4.7 Tensile stress-strain curves for three samples of CNF tabs. Each tab had a 94mm in length, 20mm in width, and 6.5mm in thickness. The results suggest CNF has a higher tensile strength than HDPE.

4.3.2. Qualitative Machining of Material

Preliminary machining of CNF solids to screws was successful. A machinist created two screws of different length, diameter, and head type which maintained ¼-20 threads. The threads, the main focus of the experiment, machined well with good material flow. Steel nuts for ¼-20 threads were spun up and down the threads multiple times, finding no snags, cross threading or deformation within the threading. It was noted the spinning nut felt as smooth as it did on a steel screw of identical thread size and pitch. The mid-processed screws with multiple test nuts can be observed in Figure 4.7. The machinist noted CNF with high porosity above 40% and micron pore

Figure 4.8 CNF fixation screws mid production. Using nuts to test the threading, it was observed CNF threads are no more resistant to movement than steel threads. No snags or cross threading were noted. Carbon burning can be noted on the block of the bottom sample. This was caused by a dull cutting blade.

sizes and below were unable to handle the stress of the threading process. Because of this CNF samples with larger, cavitated pores were removed from this experiment.

The machinist noted CNF flowed efficiently while machined. It was observed low porosity CNF mills and lathes like a hybrid of wood and a medium density polymer ($1g/cm^3$). Unlike wood, CNF will flow slightly when heated from kinetic energy. These are typical characteristic of a polymer. Unlike a polymer, however, CNF will not melt. After a quick flow phase, the CNF will begin to burn and char. A small example of this can be seen in Figure 4.8. Like wood, CNF will crack if specific stresses are put on it. This is uncharacteristic of most polymers. An example of this force would be inserting a screw too close to the materials edge, creating a blowout and failure

of the materials integrity. With these positive results, the CNC machine was the next phase in testing the physical limits of cellulose nanofibers.

CNC machining of the material yielding extremely positive results and was considered a success. As described and planned, design 1 was the CAD filed used for the procedure. 3 bone

Figure 4.9 Three samples of the CNC machined CNF bone fixation plates (design #1). The center sample contains the large cavities and 1wt% iron oxide nanoparticles. It machined with the same efficiency as the tan, standard CNF samples.

plates were to be fabricated from non-cavitated, high density CNF. While one sample of cavitated CNF was used as a side test to examine the possibilities of bone plate machining the very interesting cavitated CNF samples. The results of the experiment can be seen in Figure 4.9 in the form of completed bone fixation plates.

With the experimentation of manual and CNC machining concluding in success, the next phase of machining was implemented. Bone plate design #2 was implemented into the CNC device to test the limits of CNF capabilities. Design #2 is 1.5mm in thickness compared to the 2.3mm thickness of design #1, providing a 35% decrease. In addition, a 45 degree contour is added to the plate, providing a more challenging machining process. This contour is typical among a percentage of orthopedic fixation plates. Four bone plates were machined using the CAD file of design #2. The increased complexity of the designed required the Advanced Manufacturing Center to create a customized mount for the raw material while machining takes place.

The resulting fixation devices from the CNC process of design #2 can be seen in Figure 4.10. Qualitative examination of the fixation plates note that despite using 106% less material than design #1, the plate maintains strength and feels robust. Quantitatively it can be assumed design #2 is mechanically weaker than design #1 overall, however, design #2 is for more specific applications that require more finesse than strength. Design 2# works especially well for smaller bones such as the metacarpals of the hands, metatarsals of the feet, and the various smaller bones of the wrist and ankle.

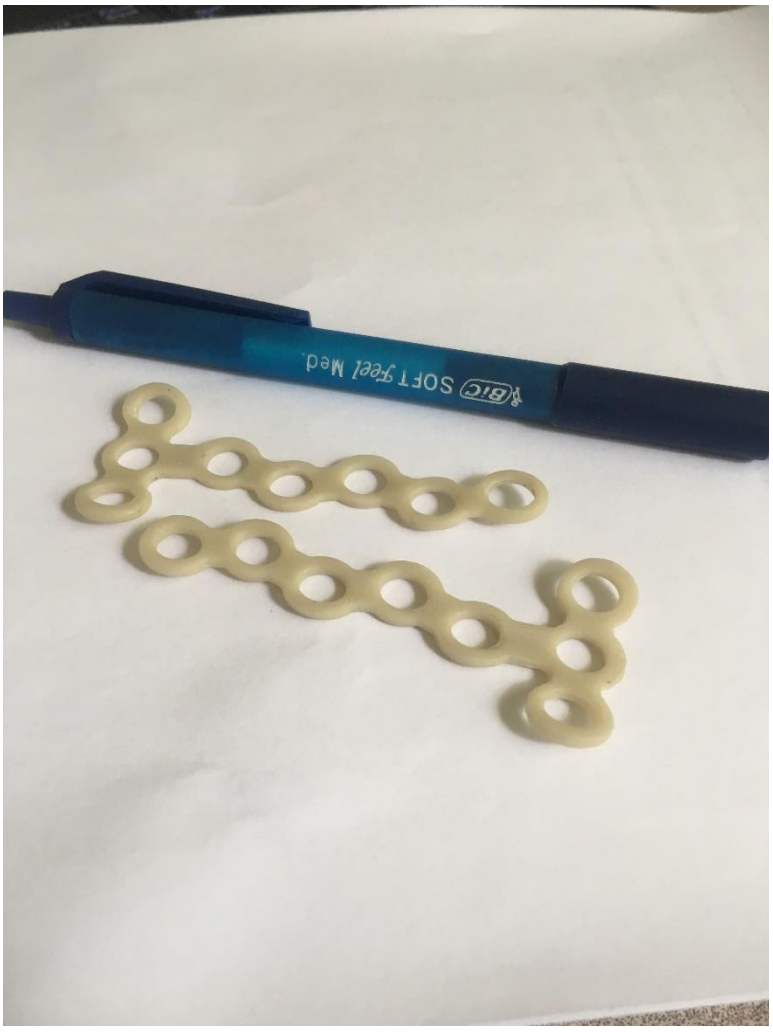

Figure 4.10 Two CNC machined CNF bone fixation plates following the more complex design #2. The plates are upside down to show their curvature to contour to bone. A pen is

4.4. Discussion

Additional mechanical testing suggests CNF is a more than capable material to use for machine processing of orthopedic implants on an industrial scale. This is specifically true of instruments such as a CNC device or an automated lathe; neither of which would require human operation. Both the tensile strength and compressive strength of CNF were comparable or better than that of HDPE, a common polymer that has highly mechinable properties. Table 2 compares CNF tensile mechanical data to known quantities of various polymers. From this table, one can

note CNF lacks the ultimate tensile strength of many of the listed polymers. This is acceptable due to the inherent biocompatibility of CNF and the ability to form stronger CNF composites. In addition, many of these strong polymers have large elongation percentages during tensile testing. This suggests the polymer has a larger chance to undergo the creep phenomena over time. Creep is a serious material flaw for an object that most withstand an orthopedic environment for a long period of time. CNF has a small elongation percentage and therefore it is suggested to have little creep occurring within the structure. When Table 4.1 is observed further it can be seen the polymers with the smallest elongation percentages have glass fiber within. The fibrous nature of CNF may provide this small elongation factor that many of the common polymers lack.

Polymer Type	Ultimate Tensile Strength (MPa)	Elongation %	Tensile Modulus (GPa)
ABS	40	30	2.3
ABS + 30% Glass Fiber	60	2	9
Acetal Copolymer	60	45	2.7
Acetal Copolymer + 30% Glass Fiber	110	3	9.5
Acrylic	70	5	3.2
Nanocellulose Fiber	**26**	**2**	**3.8**
Nylon 6	70	90	1.8
Polyamide-Imide	110	6	4.5
Polycarbonate	70	100	2.6
Polyethylene, HDPE	15	500	0.8
Polyethylene, Terephthalate (PET)	55	125	2.7
Polyimide	85	7	2.5
Polyimide + Glass Fiber	150	2	12
Polypropylene	40	100	1.9
Polystyrene	40	7	3

Table 4.1 Comparing the mechanical properties of nanocellulose fiber to various other common polymers typically used and machined in industrial settings. Features for nanocellulose fiber are highlighted in yellow.

The machinability of nanocellulose fiber is extremely promising for future orthopedic applications in the future. When Figure 4.6 is observed the stress strain curve of CNF has similar characteristics to that of human bone. This is identified by an initial linear elastic region followed by a less stiff post yield region. A direct comparison is made to Figure 4.11, showing the viscoelastic compressive stress-strain curves of human bone. The non-linear curve is noted before

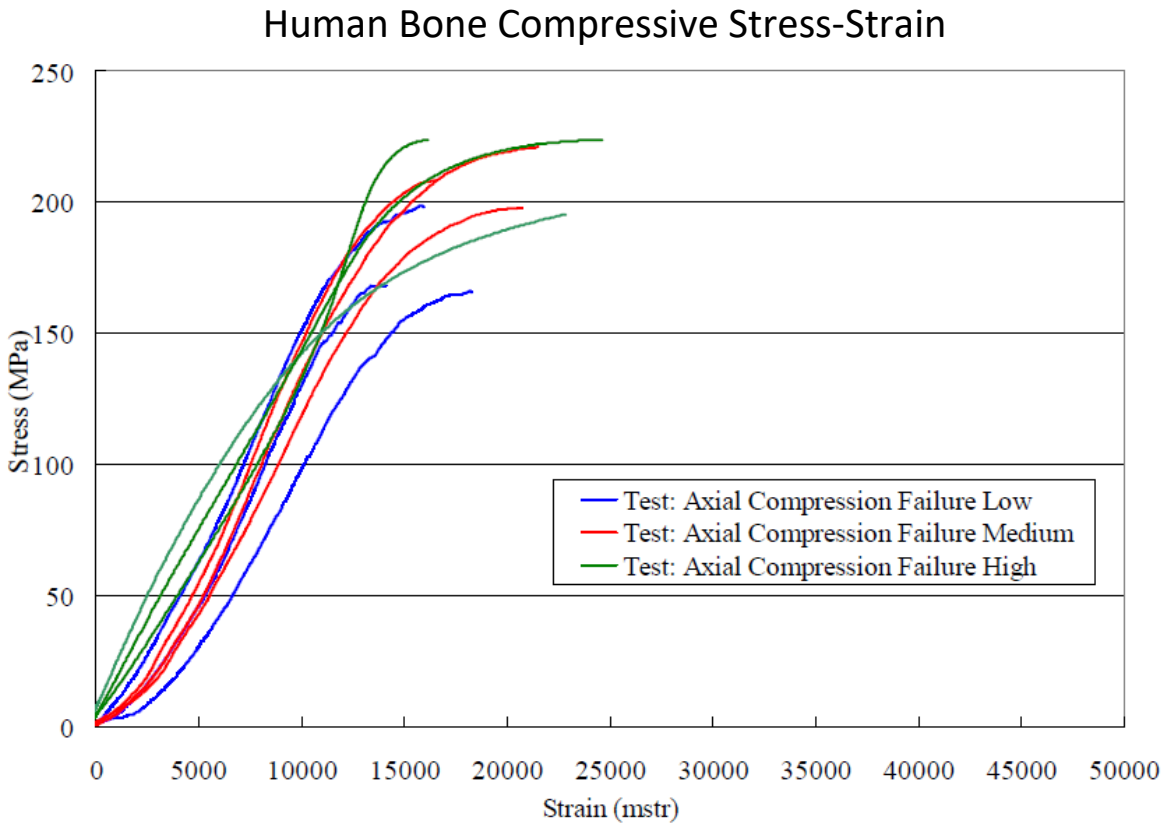

Figure 4.11 Experimental compressive stress-strain curve of human bone. Note the linear elastic region and the non-linear region of the curve directly before failure. (Ref 28)

material failure as it is noted in CNF. The major differences between bone and CNF are observed with the larger compressive strength of bone (160-225MPa) [29] and the larger plastic region in CNF compared to bone. Because CNF contains no brittle material and is a polymer this result is expected. Suggesting the viscoelastic properties of CNF are caused by the fibrous network and structure. The compressive stress-strain data within Figure 4.6 further suggests that the initial

compressive stress of CNF is comparable or better than a patented cellulose based fixation screw technology[27]. Giving further credence to the capabilities of CNF as a technology for medication orthopedic fixation application. This patented screw is a cellulose acetate-ethyl cellulose combination. The patent further covers cellulose acetate-hydroxyapatite (HA) composite materials under a wide range of ratios. Current CNF measurements are extremely similar to cellulose acetate screws made with molecular weight polymers of 50k (24MPa) and are a significant improvement (36% higher compressive strength) over cellulose acetate screws using a molecular weight of 30k.

The addition of HA to the cellulose acetate covered within the patent increases the compressive strength of the fixation screws to 35MPa, above the current limitations of pure CNF being produced at the University of Maine. However, mechanical similarities of CNF to high molecular weight cellulose acetate suggest a CNF-HA composite material will be comparable to the cellulose acetate-HA composite. This further identifies the need for hydroxyapatite experimentation with cellulose nanofibers. Further mechanical testing has shown CNF will benefit from an increase in brittle nature due to a crystalline lattice. There are multiple methods of incorporating HA into CNF, requiring all methods be examined to determine the optimal procedure and optimal material for orthopedic application. HA within CNF not only has the potential to improve mechanical strength but also improve osteocyte ingrowth.

CHAPTER 5

BONE MINERAL CNF SUPPLEMENTATION

5.1. Introduction

There are various methods to incorporate the mineral hydroxyapatite to the CNF matrix to improve mechanical strength and osteocyte biocompatibility. Osteocyte and mineral ingrowth capabilities within the CNF material require further investigation. Experimentation incorporating biomimetic growth of hydroxyapatite on the fibrils within SPF is a satisfactory examination of ingrowth of bone based minerals such as HA. The magnitude of apatite layer formation is a preliminary confirmation CNF has the ability to integrate with native bone. As stated previously, bone tissue ingrowth is a primary characteristic of any material that can form a bone fixation device capable of self-dissolution *in vivo*. The ability to control dissolution rates of CNF and in-growth rates of osteocytes will be a major focus of study moving forward. Experimentation will be done incorporating HA into CNF to attempt a biomimetic composite.

5.2. Methods

The initial method of action is to attempt HA crystal growth on CNF fibers within a three dimensional matrix. Research has shown that nanocellulose fiber with a phosphorylated surface create more nucleation sites for hydroxyapatite crystal formation.[21] These findings suggest any experiment growing HA on CNF should be done on a phosphorylated and non-phosphorylated CNF produced at the University of Maine. Physical differences between UM CNF and electro spun CNF may cause a difference in the phosphorylation affect. An 85% porosity CNF matrix was selected for the growth experiment. Despite the concern of mass transport limitation caused by the 1-5 micron pores typical of this porosity; the possibility of creating a CNF-HA composite rod

with the same HA content as bone was too exciting to not attempt. If issues arose within the experiment in terms of mass transport then a later experiment would correct these.

Following literature, to phosphorylate the CNF surface a phosphorylating solution was initially produced. 200ml of phosphoric acid (H_3PO_4), 200ml of ethanol, and 250ml of hexanol were added to a 2L beaker at 35˚C under agitation of a magnetic stir bar. 62.5g of phosphorous pentoxide (P_2O_5) was added to the solution and stirred for 24 hours[22]. Simultaneously, 85% porosity freeze dried CNF rods of 10mm diameter were added to 200ml of ethanol and 250ml of hexanol to pre-soak for 24 hours[21]. Once the phosphorylating solution was uniformly mixed and clear, the CNF rods were transferred to soak and phosphorylate for 72 hours. Once complete the rods were soaked in DI water for 12 hours and later rinsed in DI water to remove any remaining acid or solvent. The rods were then lyophilized for 24 hours. Phosphorylation of the rods were never measured as this was a first generation, preliminary experiment. The experimental assumption was made that increases in fiber phosphorylation, or lack thereof, would be observable through the growth of HA on the fibers. In the future, XPS (X-ray photoelectron spectroscopy) will be used to measure P_2 on the fiber surface.

Following the same literature, with phosphorylated and non-phosphorylated porous CNF rods produced, SBF for growing HA was prepared in 2L batches. 15.5801g of sodium chloride, 0.07057g sodium hydrogen carbonate, 0.4259g disodium hydrogen phosphate, and 0.6099g of magnesium chloride hexahydrate were added to a beaker with 1700ml DI water. The pH of the SBF was measured and adjusted to 7.4 using 1M hydrochloric acid (HCl). 0.8325g of anhydrous calcium chloride and 0.1420g of sodium sulfate were added to the solution. The SBF was completed by adjusting the pH value back to 7.4 using TRIS, a well-known buffer, and adjusting

the final volume of SBF to 2000ml using DI water. The SBF was agitated under magnetic stirring and heated to 37˚C[22].

The Phosphorylated CNF rods (PCNF) were placed into the SBF to soak for 14, 21, and 28 days, changing the SBF solution every 24 hours. Additionally, standard CNF rods were added as a control group and removed at the same times as PCNF to test the effect of phosphorylation alone. When rods were removed they were rinsed with DI water and lyophilized for 48 hours.

5.3. Results

Because 85% porous CNF and HA look the same to the human eye and are both stark white in color, more complex means were needed than qualitative observation to confirm how HA grew on the CNF surfaces. The rods were broken by hand to prevent smearing from a tool or blade

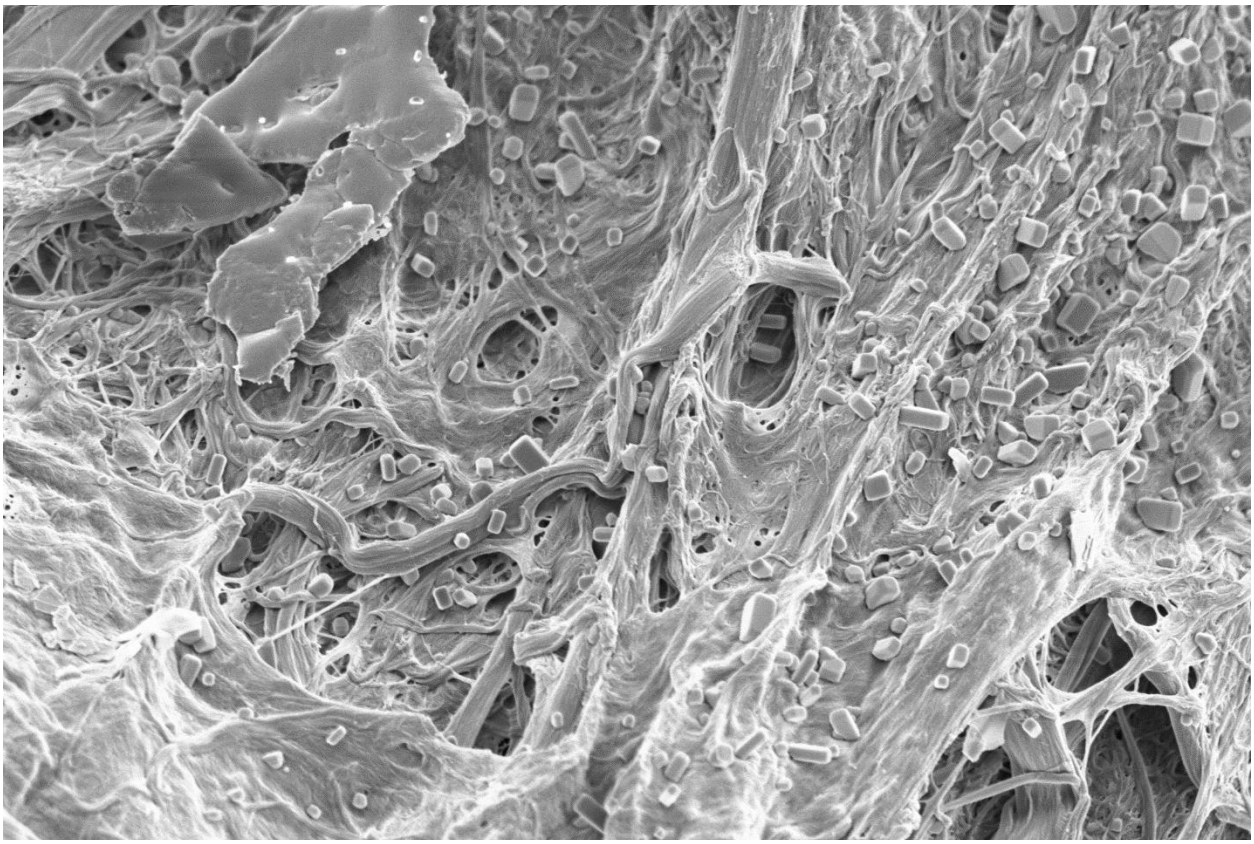

Figure 5.1 SEM image showing crystal formation within the CNF matrix of the rod. 5K x magnification

and to access the cross sectional interface. A cross sectional view is needed to determine mass transport of HA and growth into the rod. SEM images were taken of these cross sections after being sputter coated in silver. It was found that the majority of samples, both CNF and PCNF had no noticeable hydroxyapatite within the cross section of the rod. However, as can be seen in Figure 5.1, one 28 day PCNF sample was found to have what appear to be nucleation crystals in the center.

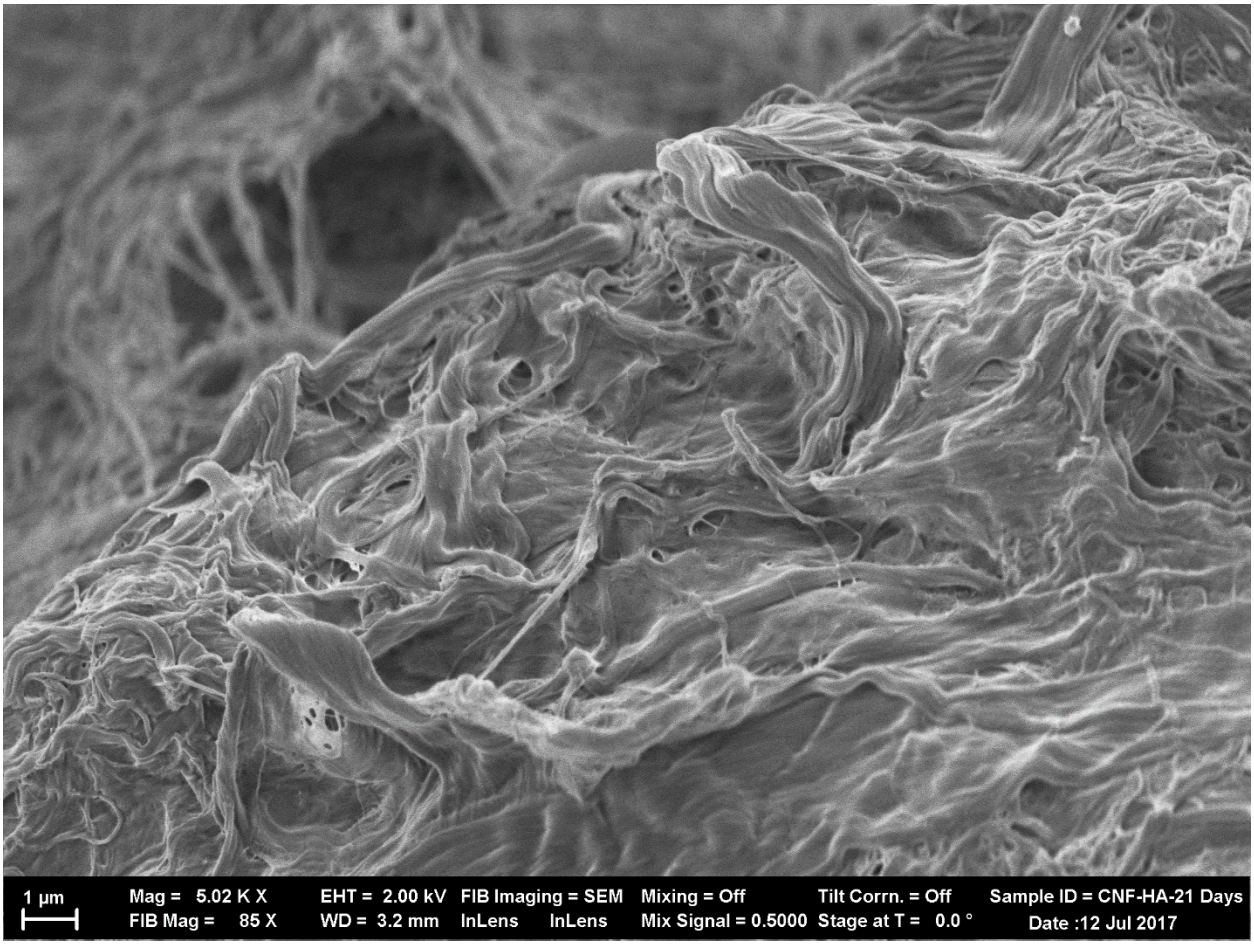

Figure 5.2 PCNF SEM image showing no crystals on the fiber surface. This image represents the remaining population of samples. 5k x magnification.

Closer observation of Figure 5.1 suggests the crystal structures are growing off and out of the fiber and not past precipitates resting on top of the matrix. Figure 5.2 is used as a reference for PCNF with no inside crystals, under 28 days of SBF growth, at the same magnification of 5k. Figure 5.2 is an excellent representation of the population of SEM images for both CNF and PCNF. When the image is lowered in magnification to 750X in Figure 5.3 the consistent spread of the crystals is easily observed throughout much of the fiber bed. Some crystals within Figure 5.2 are small and can be missed on first inspection. The top right of the image reveals the crystals best.

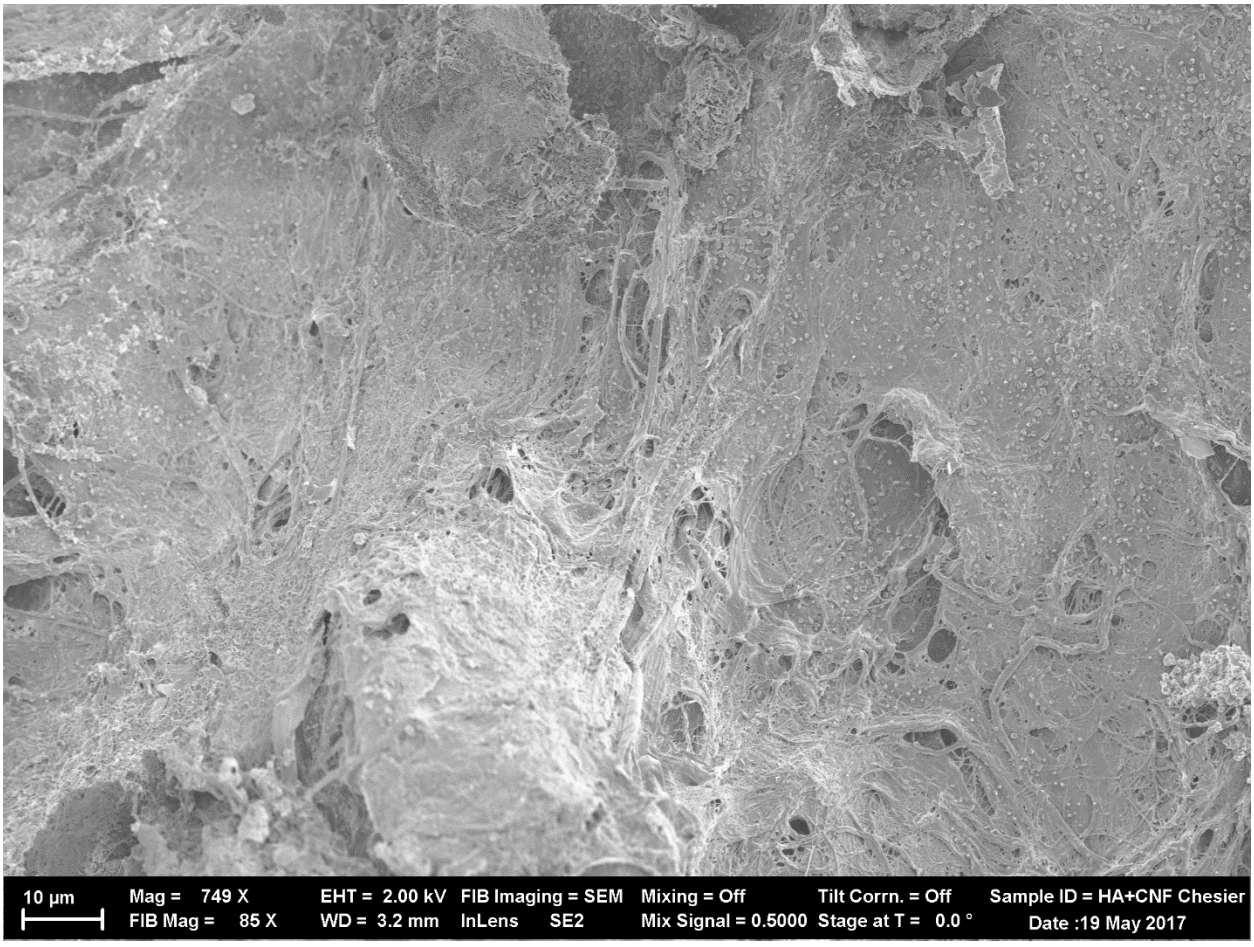

Figure 5.3 SEM image of widespread crystallization across the CNF bed within the rod. 750 x magnification

Because little hydroxyapatite was found within the rods focus of observation focused to the rod surface. Qualitative testing of the rod surface with a metal scarping tool suggested hydroxyapatite was present; as the metal, tool created a high pitched sound while being abraded with the tool. Pure CNF typically makes no sound when abraded. SEM images were taken of the rod surface. All images had a similar appearance to Figure 5.3, a mature HA crystal formation consisting of many thin plates. These crystals appear different from the proposed nucleation crystals because crystal lattices can changed overtime as the lattice grows upon itself.

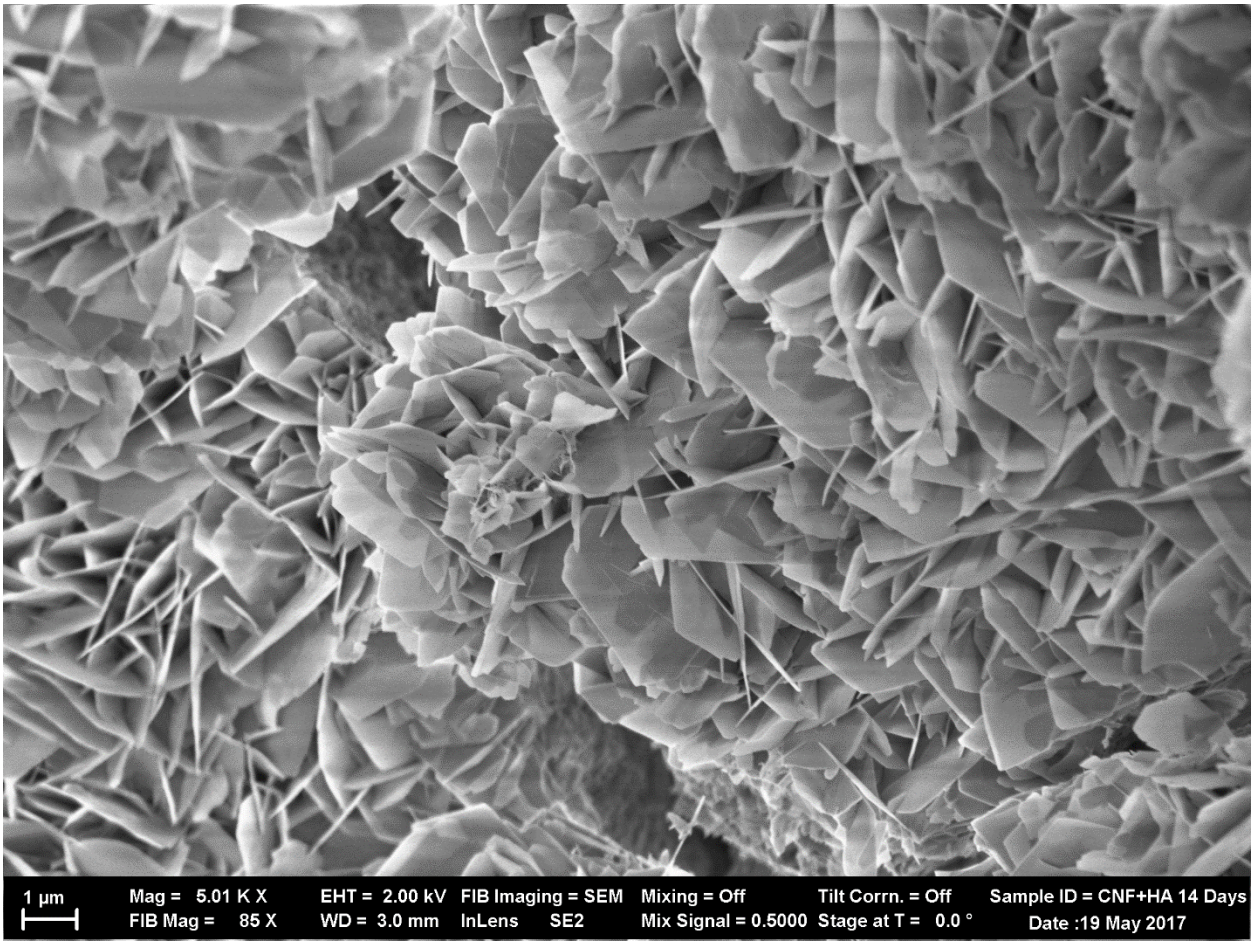

Figure 5.4 Hydroxyapatite crystal structure on the surface of the CNF rod. 5K x magnification

Further SEM images were taken at lower magnitude of the HA-CNF interfaces within the cross section of the rod. Attempts at proper contrast were difficult. However, one can observe in Figure 5.4 the clusters of the HA macrostructure growing atop the CNF. The fibers in the center and bottom of the image are clearly visible, even when out of the focal plane. Multiple cluster of HA can be viewed growing within and on the fibrous matrix after the rod was broken open.

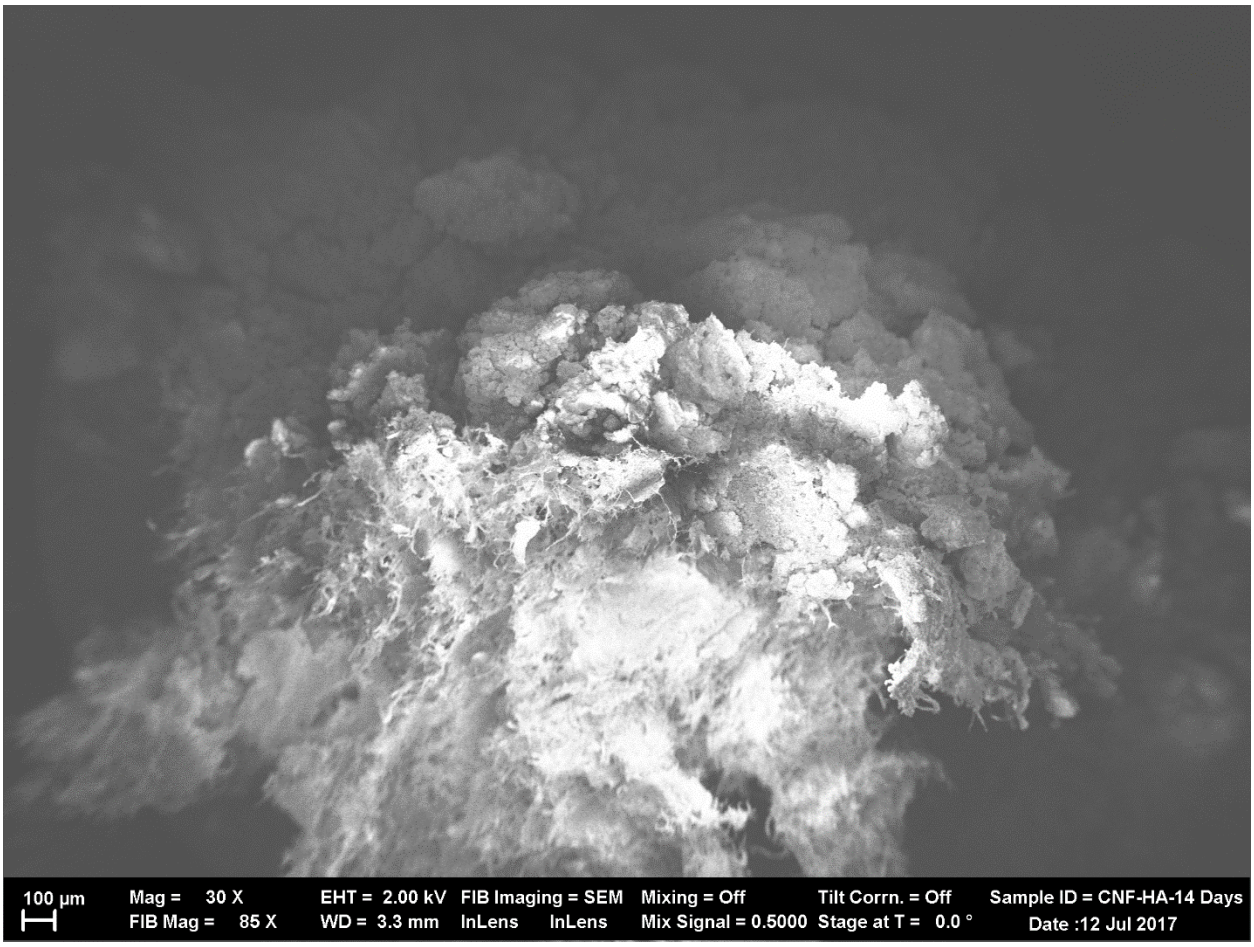

Figure 5.5 Macro structure of HA crystals growing on and within the CNF fibrous matrix from the outside in. 30 x magnification

These SEM imaging helps confirm that the majority of the HA growth within the SBF fluid occurred on the surface of the rod and continuously grew outwards and built upon itself. Blocking any mass transport of minerals to the center of the fibrous rod.

5.4. Discussion

As stated previously, mass transport limitations limited the success of this experiment. With CNF pores of 1 micro, HA growth rapidly sealed the pores. The sealing of the pores prevented ingredients within the SBF to transport within the fibrous matrix of the rod to induce nucleation growth. This was the case for both CNF and PCNF samples, and for the 14, 21, and 28 day samples as well. However, the experiment suggests growth of hydroxyapatite on CNF produced by the University of Maine is achievable. Unfortunately, the nature of the experimental results gives no information of CNF versus PCNF HA growth performance; as the majority of HA was building upon itself and not cellulose nanofiber

A new experiment will need to be run, this time maximizing surface area and using freeze dried CNF with a porosity of 97%. Most ideally a thin square chip or thin disk, 1-3mm in thickness. This increased porosity should increase mass transport of HA producing compounds into the matrix by providing larger pores. These pores will be in the 100 micron range and will not be clogged by HA growth as fast as the 1 micron pores. The thin width of the chip or disk will decrease the distance the compounds will need to diffuse overall. A diffusion distance of 0.5mm will be a 1000% decrease over the 5mm radius of the rod. A better executed experiment will provide greater information and may confirm or deny the need for phosphorylated nanocellulose fiber going forward with osteoblast/CNF research.

CHAPTER 6

CONCLUSIONS

As technology advances greater problems in the medical industry will look to be solved in increasingly novel ways. The lack of an acceptable bone analog; using materials that fail to match the unique Young's modulus of bone, physical, and mechanical properties has created suboptimal conditions in the orthopedic field since its inception. A unique material solution has been presented from nature in the form of nanocellulose fiber. Poetically and fittingly derived from trees; another living being.

Experimentation on pure cellulose nanofibers has suggested CNF has a place as a biodegradable plastic for both orthopedic and biomedical application. A methodology to dewater cellulose nanofiber slurries in a rapid, controlled manner was developed. Large solid form CNF ingots were produced and machined. Mechanical tunability was suggested via porosity control of the end product. The maximum Young's modulus (6GPa), max yield stress (100MPa), compressive strength (30MPa), and tensile strength (25MPa) were determined with an INSTRON device. Suggesting CNF is comparable mechanically to PLA and collagen. Orthopedic fixation screws and plates were fabricated from CNF ingots. It was determined orthopedic machinability of the material was satisfactory. Both a lathe and CNC device were used to create plates and screws that mimic current orthopedic technology. Preliminary trials to grow hydroxyapatite on CNF were run. Results were inconclusive because of flaws within the experimental design. Corrections to the experimental design will be implemented and practiced for future HA studies.

The majority of future work for CNF medical application is HA ingrowth, Osteoblast ingrowth, and composite experimentation. CNF has respectable mechanical properties that mimic

dense collagen, 20% of bone mass. However, the strong, brittle mechanical properties HA provides are unaccounted for. Because human bone is a composite of two materials providing mechanical strength, biomimetic techniques should be used to attempt a synthetic, CNF-HA, bone composite. This method is currently preformed to produce HA-molded polymer composites for fixation screws. However, these materials struggle to match the overall Young's modulus and strength of bone; requiring HA to provide the majority of support. It is shown CNF is mechanically superior to the majority of biodegradable polymers and comparable to the others. A successful composite should bring significant results.

An orthopedic fixation material that does not biodegrade and resorb within the body suboptimal and can always cause complications or secondary surgeries. A fixation screw that leaves a hole within the bone structure of a patient after resorption is even less suboptimal. Osteoblast ingrowth experiments will be done within three dimensional matrices of CNF and HA-CNF to compare cell viability and the affect HA has, if any, on osteoblast chemotaxis. Bone ingrowth capabilities will be essential for CNF acceptance within the biomedical field. This thesis suggests more biomedical studies on cellulose nanofibers be done.

REFERENCES

1. Habibi, Y.; Lucia, L. A.; Rojas, O. J. Chem. Rev. 2010, 110, 3479.

2. Miyamoto T, Takahashi S, Ito H, Inagaki H, Noishiki Y. Tissue biocompatibility of cellulose and its dervivatives. J Biomed Mater Res 1989;23:125-33.

3. Martson M, Viljanto J, Hurme T, Laippala P, Saukko P. Is cellulose sponge degradable or stable as implantation material? An in vivo subcutaneous study in the rat. Biomaterials 1999;20:1989-95

4. T. Albrektsson, P.-I. Branemark, H.-A. Hansson, and J. Lindstrom, "Osseointegrated titanium implants. Requirements for ensuring a long-lasting, direct bone-to-implant anchorage in man," Acta Orthopaedica Scandinavica, vol. 52, no. 2, pp. 155–170, 1981. View at Publisher · View at Google Scholar · View at Scopus

5. T. Albrektsson and A. Wennerberg, "The impact of oral implants—past and future, 1966–2042," Journal of the Canadian Dental Association, vol. 71, no. 5, pp. 327–327, 2005. View at Google Scholar · View at Scopus

6. Dalal, A., Pawar, V., Mcallister, K., Weaver, C., & Hallab, N. J. (2012). Orthopedic implant cobalt-alloy particles produce greater toxicity and inflammatory cytokines than titanium alloy and zirconium alloy-based particles in vitro, in human osteoblasts, fibroblasts, and macrophages. *Journal of Biomedical Materials Research Part A, 100A*(8), 2147-2158. doi:10.1002/jbm.a.34122

7. Liu, Naicheng, Jia Meng, Zhenheng Wang, Gang Zhou, Tongguo Shi, and Jianning Zhao. "Autophagy Mediated TiAl6V4 Particle-induced Peri-implant Osteolysis by Promoting Expression of TNF-α." *Biochemical and Biophysical Research Communications* 473.1 (2016): 133-39. Web.

8. Ratner, B. D. (2004). *Biomaterials science: An introduction to materials in medicine*. Amsterdam: Elsevier Academic Press.

9. Bandyopadhyay, A., Espana, F., Balla, V. K., Bose, S., Ohgami, Y., & Davies, N. M. (2010). Influence of Porosity on Mechanical Properties and *In vivo*Response of Ti6Al4V Implants. *Acta Biomaterialia*, *6*(4), 1640–1648. http://doi.org/10.1016/j.actbio.2009.11.011

10. Jorfi, M., & Foster, E. J. (2014). Recent advances in nanocellulose for biomedical applications. *Journal of Applied Polymer Science,132*(14). doi:10.1002/app.41719

11. Vartiainen J, Pohler T, Sirola K, Pylkkanen L, Alenius H, Hokkinen J, et al. Health and environmental safety aspects of friction grinding and spray drying of microfibrillated cellulose. Cellulose 2011;18:775–86.

12. Hannukainen K-S, Suhonen S, Savolainen K, Norppa H. Genotoxicity of nanofibrillated cellulose in vitro as measured by enzyme comet assay. Toxicol Lett 2012;211:S1–S174.

13. Norppa H. Nanofibrillated cellulose: results of in vitro and in vivo toxicological assays. Presentation on Sunpap conference 2012. <http://sunpap.vtt.fi/pdf/final_conference/13_SUNPAP_Norppa_2012.pdf>.

14. Vaananen V, Rydman E, Ilves M, Hannukainen K, Norppa H, von Wright A, et al. Evaluation of the suitability of the developed methodology for nanoparticle health and safety studies. Sunpap conference; 2012. <http://sunpap.vtt.fi/pdf/SUNPAP_WP10_DEL10_5_20120827_FIOH.pdf>.

15. Alexandrescu L, Syverud K, Gatti A, Chinga-Carrasco G. Cytotoxicity tests of cellulose nanofibril-based structures. Cellulose 2013;20:1765–75.

16. Pereira, M. M., Raposo, N. R., Brayner, R., Teixeira, E. M., Oliveira, V., Quintão, C. C., . . . Brandão, H. M. (2013). Cytotoxicity and expression of genes involved in the cellular stress response and apoptosis in mammalian fibroblast exposed to cotton cellulose nanofibers. *Nanotechnology,24*(7), 075103. doi:10.1088/0957-4484/24/7/075103

17. Hua K, Carlsson DO, Alander E, Lindstrom T, Stromme M, Mihranyan A, et al. Translational study between structure and biological response of nanocellulose from wood and green algae. RSC Adv 2014;4:2892–903.

18. Hadjizadeh, A., & Doillon, C. J. (2010). Directional migration of endothelial cells towards angiogenesis using polymer fibres in a 3D co-culture system. *Journal of Tissue Engineering and Regenerative Medicine, 4*(7), 524–531. https://doi.org/10.1002/term

19. Nimeskern L, Avila HM, Sundberg J, Gatenholm P, Muller R, Stok KS. Mechanical evaluation of bacterial nanocellulose as an implant material for ear cartilage replacement. J Mech Behav Biomed 2013;22:12–21.

20. Lopes JL, Machado JM, Castanheira L, Granja PL, Gama FM, Dourado F, et al. Friction and wear behaviour of bacterial cellulose against articular cartilage. Wear 2011;271:2328–33.

21. Gefen, A. (2002). Computational simulations of stress shielding and bone resorption around existing and computer-designed orthopaedic screws. *Medical & Biological Engineering & Computing,40*(3), 311-322. doi:10.1007/bf02344213

22. Shady Farah, Daniel G. Anderson, Robert Langer, Physical and mechanical properties of PLA, and their functions in widespread applications — A comprehensive review, Advanced Drug Delivery Reviews, Volume 107, 2016, Pages 367-392, ISSN 0169-409X, http://dx.doi.org/10.1016/j.addr.2016.06.012.

23. J. Russias, E. Saiz, R.K. Nalla, K. Gryn, R.O. Ritchie, A.P. Tomsia, Fabrication and mechanical properties of PLA/HA composites: A study of in vitro degradation, Materials Science and Engineering: C, Volume 26, Issue 8, 2006, Pages 1289-1295, ISSN 0928-4931, http://dx.doi.org/10.1016/j.msec.2005.08.004.

24. Li, K., Wang, J., Liu, X., Xiong, X., & Liu, H. (2012, July 6). Biomimetic growth of hydroxyapatite on phosphorylated electrospun cellulose nanofibers. *Carbohydrate Polymers,90*(4), 1573-1581. doi:10.1016/j.carbpol.2012.07.033

25. Chen YM, Xi T, Zheng Y, Guo T, Hou J, Wan Y, et al. In vitro cytotoxicity of bacterial cellulose scaffold for tissue engineered bone. J Bioact Compat Polym 2009;24:137–45.

26. Jeong SI, Lee SE, Yang H, Jin YH, Park CS, Park, et al. Toxicologic evaluation of bacterial synthesized cellulose in endothelial cells and animals. Mol Cell Toxicol 2010;6:373–80.

27. Kim G-D, Yang H, Park HR, Park C-S, Park YS, Lee SE. Evaluation of immunoreactivity of in vitro and in vivo models against bacterial synthesized cellulose to be used as a prosthetic biomaterial. BioChip J 2013;7:201–9.

28. Lee K-Y, Buldum G, Mantalaris A, Bismarck A. More than meets the eye in bacterial cellulose: biosynthesis, bioprocessing, and applications in advanced fiber composites. Macromol Biosci 2014;14:10–32.

29. Sugawara, Y; Kamioka, H; Honjo, T; Tezuka, K; Takano-Yamamoto, T (2005). "Three dimensional reconstruction of chick calvarial osteocytes and their cell processes using confocal microscopy". *Bone*. **36** (5): 877–83. doi:10.1016/j.bone.2004.10.008.

30. Sangamesh G. Kumbar, inventor, Cato T. Laurencin, inventor, University of Connecticut, assignee, Natural Polymer-Based Porous Orthopedic Fixation Screw for Bone Repair and Regeneration. US Patent 20,110,208,190 A1. August 25th, 2011

31. Andrew Kemper, Craig McNally, Eric Kennedy, Sarah Manoogian, Stefan Duma, THE MATERIAL PROPERTIES OF HUMAN TIBIA CORTICAL BONE IN TENSION AND COMPRESSION: IMPLACATIONS FOR THE TIBIA INDEX, Virginia Tech – Wake Forest, Center for Injury Biomechanics United States, Paper Number 07-0470

BIOGRAPHY OF THE AUTHOR

The author was born in the spring of 1991 in East Norwalk, Connecticut. He attended Norwalk High School where he was a member of the chambers singers and the traveling choir. Shortly after graduating high school in May 2009 he moved to Orono, Maine to begin his undergraduate degree in Bioengineering. While attending the University of Maine he found the art of hip hop dance and became a key member of hip hop performances on campus for 4 years. After graduating in 2014 with his Bachelors of Science degree in Bioengineering, he chose to further his education at the same university and department he grew up in for 5 years prior. He is a candidate for a Master of Science degree in Biological Engineering from the University of Maine in August 2017.